METHODS

Plasmids and reagents. cDNA clones encoding mouse IGFBPs and *Xenopus* IGFBP-4 were purchased from Open Biosystems. XIGFBP-4-H74P mutant was generated with a QuickChange Site-Directed Mutagenesis kit (Stratagene). His-tagged human wild-type IGFBP-4 and mutant IGFBP-4-H74P (vectors provided by X. Qin)[8] were produced and purified with HisTrap HP Kit (Amersham). Full-length Frz8, Frz8CRD and LRP6N were provided by X. He[22,23]. Full-length LRP6, membrane-bound forms of LRP6 deletion mutants, and Dkk1 were from C. Niehrs[24]. pXwnt8 and pCSKA-Xwnt8 were from J. Christian[25]. pCS2–β-catenin was from D. Kimelman[26]. αMHC–GFP was from B. Fleischmann[27]. BRE–luc was from P. ten Dijke[28]. pCGN-Dvl-1 was described previously[29]. Soluble forms of LRP6 deletion mutants and probes for *in situ* hybridization analysis (Nkx2.5, cTnI and Hex) were generated by PCR. IGFBP-4, Wnt3A, IGF-I, IGF-II and BMP2 were from R&D. Neutralizing antibodies were from R&D (anti-IGFBP-4), Sigma (anti-IGF-I and anti-IGF-II), and Oncogene (anti-type-I IGF receptor). The antibodies used for immunoprecipitation, western blotting and immunostaining were from Invitrogen (anti-Myc, anti-V5), Santa Cruz (anti-cTnT, anti-IGFBP-4, anti-topoisomerase I (TOPO-I)), Sigma (anti-β-actin, anti-β-catenin, anti-FLAG (M2)) and Developmental Studies Hybridoma Bank (anti-sarcomeric myosin heavy chain (MF20)).

Cell culture experiments. P19CL6 cells and ES cells were cultured and induced to differentiate into cardiomyocytes essentially as described[8,30]. P19CL6 cells (2,000 cells per 35-mm dish) were treated with various conditioned media for screening of their cardiogenic activities. P19CL6 cells or ES cells stably transfected with αMHC promoter driven–GFP were generated by transfection of αMHC–GFP plasmid into P19CL6 cells or ht7 ES cells followed by G418 selection. Luciferase reporter gene assays, western blot analyses, immunostaining and RT–PCR were performed as described[30]. Reporter gene assays were repeated at least three times. PCR primers and PCR conditions are listed in Supplementary Table 1. For siRNA-mediated knockdown, siRNAs were expressed with pSIREN-RetroQ vector (Clontech). Oligonucleotide sequences used are listed in Supplementary Table 2. pSIREN-RetroQ vectors ligated with double-stranded oligonucleotides were transfected into P19CL6 cells or ES cells, and puromycin-resistant clones were isolated and expanded. For β-catenin stabilization assays, nuclear extracts of L cells were prepared with NE-PER Nuclear and Cytoplasmic Extraction Reagents (Pierce). Data are shown as means and s.d.

IP/western blot analyses and binding assays. Conditioned media for IP/western blot analyses containing full-length or various deletion mutants of IGFBPs, LRP6, Frz8CRD and Dkk1 were produced with 293 cells. Binding reactions were performed overnight at 4 °C. Immunoprecipitation was performed with Protein G–Sepharose 4 Fast Flow (Amersham). ^{125}I-labelling of IGFBP-4 and Wnt3A was performed with IODO-BEADS Iodination Reagent (Pierce). A liquid-phase binding assay was performed essentially as described[19]. In brief, conditioned media containing LRP6N–Myc or Frz8CRD–Myc were mixed with various concentrations of ^{125}I-labelled IGFBP-4 and incubated overnight at 4 °C. LRP6N–Myc or Frz8CRD–Myc was immunoprecipitated and the radioactivity of bound IGFBP-4 was measured after extensive washing of the Protein G–Sepharose beads. For a competitive binding assay, conditioned media containing LRP6N–Myc or Frz8CRD–Myc were mixed with ^{125}I-labelled Wnt3A and unlabelled IGFBP-4, and incubated overnight at 4 °C. LRP6N–Myc or Frz8CRD–Myc was then immunoprecipitated and the radioactivity of bound Wnt3A was measured.

***Xenopus* experiments and mouse *in situ* hybridization analysis.** Axis duplication assays, animal cap assays and *in situ* hybridization analyses in *Xenopus* were performed essentially as described[20]. Two independent cDNAs for *XIGFBP-4*, presumably resulting from pseudotetraploid genomes, were identified by 5′ rapid amplification of cDNA ends (Supplementary Fig. 4a). Two different MOs targeting both of these two IGFBP-4 transcripts were designed (Gene Tools) (Supplementary Fig. 4a and Supplementary Table 2). MO-sensitive *XIGFBP-4* cDNA including a 41-base-pair 5′-untranslated region (UTR) was generated by PCR. MO-resistant *XIGFBP-4* cDNA (wild-type and H74P mutant) was generated by introducing five silent mutations in the MO1 target sequence and excluding the 5′-UTR (Supplementary Fig. 4a). To determine the specificity of MOs, MO-sensitive or MO-resistant *XIGFBP-4–myc* mRNA was injected into *Xenopus* embryos with or without MOs, and protein/mRNA expression was analysed. PCR primers and PCR conditions are listed in Supplementary Table 1. MOs and plasmid DNAs were injected at the eight-cell stage into the dorsal region of two dorsal–vegetal blastomeres fated to be heart and liver anlage. Electroporation of mRNA was performed essentially as described[21]. Injection of mRNA (5 ng in 5 nl of solution) into the vicinity of heart anlage and application of electric pulses were performed at stage 28. Whole-mount *in situ* hybridization analysis of murine IGFBP-4 was performed as described[30].

22. He, X. *et al.* A member of the Frizzled protein family mediating axis induction by Wnt-5A. *Science* **275**, 1652–1654 (1997).
23. Tamai, K. *et al.* LDL-receptor-related proteins in Wnt signal transduction. *Nature* **407**, 530–535 (2000).
24. Mao, B. *et al.* LDL-receptor-related protein 6 is a receptor for Dickkopf proteins. *Nature* **411**, 321–325 (2001).
25. Christian, J. L. & Moon, R. T. Interactions between Xwnt-8 and Spemann organizer signaling pathways generate dorsoventral pattern in the embryonic mesoderm of *Xenopus*. *Genes Dev.* **7**, 13–28 (1993).
26. Yost, C. *et al.* The axis-inducing activity, stability, and subcellular distribution of β-catenin is regulated in *Xenopus* embryos by glycogen synthase kinase 3. *Genes Dev.* **10**, 1443–1454 (1996).
27. Kolossov, E. *et al.* Identification and characterization of embryonic stem cell-derived pacemaker and atrial cardiomyocytes. *FASEB J.* **19**, 577–579 (2005).
28. Korchynskyi, O. & ten Dijke, P. Identification and functional characterization of distinct critically important bone morphogenetic protein-specific response elements in the Id1 promoter. *J. Biol. Chem.* **277**, 4883–4891 (2002).
29. Kishida, M. *et al.* Synergistic activation of the Wnt signaling pathway by Dvl and casein kinase Iε. *J. Biol. Chem.* **276**, 33147–33155 (2001).
30. Hosoda, T. *et al.* A novel myocyte-specific gene Midori promotes the differentiation of P19CL6 cells into cardiomyocytes. *J. Biol. Chem.* **276**, 35978–35989 (2001).

nature
cell biology

A crucial role of a high mobility group protein HMGA2 in cardiogenesis

Koshiro Monzen[1,9], Yuzuru Ito[2,9], Atsuhiko T. Naito[3,9], Hiroki Kasai[1], Yukio Hiroi[1], Doubun Hayashi[1,4], Ichiro Shiojima[3], Tsutomu Yamazaki[5], Kohei Miyazono[6], Makoto Asashima[2,7,8], Ryozo Nagai[1] and Issei Komuro[3,10]

The high mobility group (HMG) of nuclear proteins regulates expression of many genes through architectural remodelling of the chromatin structure, and formation of multiprotein complexes on promoter/enhancer regions. This leads to the active transcription of their target genes[1–3]. Here we show that HMGA2, a member of the HMGA sub-family of HMG proteins, has a critical function in cardiogenesis. Overexpression of *HMGA2* enhanced, whereas siRNA-mediated knockdown of *HMGA2* blocked, cardiomyocyte differentiation of the embryonal carcinoma cell line P19CL6. Moreover, overexpression of a dominant-negative HMGA2 or morpholino-mediated knockdown of HMGA2 expression blocked normal heart formation in *Xenopus laevis* embryos, suggesting that HMGA2 has an important role in cardiogenesis both *in vitro* and *in vivo*. Mechanistically, HMGA2 associated with Smad1/4 and showed synergistic trans-activation of the gene for a cardiac transcription factor Nkx2.5; a conserved HMGA2 binding site was required for the promoter activity of *Nkx2.5* gene, both in P19CL6 cells and in transgenic *Xenopus* embryos. Thus, HMGA2 is a positive regulator of *Nkx2.5* gene expression and is essential for normal cardiac development.

The process of vertebrate heart development is regulated by a network of multiple transcription factors and signalling proteins[4,5]. Congenital heart malformations occur in approximately 1% of the population[6]; this high susceptibility of the developing heart to diseases may be in part due to the complexity of the molecular framework that controls cardiogenesis. A precise understanding of the causes of heart malformations is therefore imperative for establishing therapeutic strategies for congenital heart diseases. Molecules involved in the early stage of cardiac development are of particular interest because they may also function in repair or regeneration of the injured heart[7]. In this regard, cardiac transcription factors such as Nkx2.5 (**A001667**), GATA-4 (**A001029**) and MEF2C (**A001503**) have been investigated extensively, because they are essential for normal heart development and they are also encoded by early cardiac marker genes expressed in the heart-forming region, when cardiac precursors are specified in the anterior lateral mesoderm[5]. Signalling molecules such as bone morphogenetic proteins (BMPs), fibroblast growth factors, Wnts and soluble Wnt inhibitors have also been characterized as inducers or inhibitors of cardiac mesoderm specification[5,7]. However, it is not clear how these signalling molecules and transcription factors regulate the commitment of undifferentiated mesodermal cells into cardiac precursors.

To further investigate the regulatory mechanisms that control the early stage of cardiomyocyte differentiation, we used P19CL6 cells, which are derived from P19 murine embryonal carcinoma cell lines and differentiate into beating cardiomyocytes in the presence of 1% dimethyl sulphoxide (DMSO)[8]. Differential mRNA display was performed to isolate mRNA species whose expression was upregulated in the early stage (day 6) of P19CL6 differentiation into cardiomyocytes, when early cardiac marker genes, such as *Nkx2.5*, start to be expressed. Among the 50 clones isolated, five were confirmed by northern blotting to be upregulated at day 6 of differentiation and one of these five clones was found to be a cDNA encoding the HMG protein HMGA2. Northern blot analysis revealed that the expression of *HMGA2* mRNA was detected from day 2 and peaked at day 6 after DMSO treatment (Fig. 1a), indicating that the expression of *HMGA2* precedes those of early cardiac marker genes during cardiomyocyte differentiation.

HMGA2 is a member of the HMG superfamily of non-histone chromatin proteins, which consists of three sub-families, HMGA, HMGB and HMGN[1,3]. HMG proteins modulate the expression of many genes by remodelling the chromatin architecture and promoting the formation of multiprotein complexes on the promoter/enhancer region, leading to the active transcription of their target genes. The HMGA sub-family consists of four members, HMGA1a–c,

[1]Department of Cardiovascular Medicine, [4]Translational Research for Healthcare and Clinical Science, [5]Clinical Bioinformatics, and [6]Molecular Pathology, Graduate School of Medicine, the University of Tokyo, 7-3-1 Hongo, Bunkyo-ku, Tokyo 113-8655, Japan. [2]ICORP Organ Regeneration Project, Japan Science and Technology Agency (JST), 3-8-1 Komaba, Meguro-ku, Tokyo 153-8902, Japan. [3]Department of Cardiovascular Science and Medicine, Chiba University Graduate School of Medicine, 1-8-1 Inohana, Chuo-ku, Chiba 260-8670, Japan. [7]Department of Life Science (Biology), Graduate School of Arts and Sciences, the University of Tokyo, 3-8-1 Komaba, Meguro-ku, Tokyo 153-8902, Japan. [8]Organ Development Research Laboratory, National Institute of Advanced Industrial Sciences and Technology (AIST), Tsukuba Central 4, 1-1-1 Higashi, Tsukuba, Ibaraki 305-8562, Japan.
[9]These authors contributed equally to this work.
[10]Correspondence should be addressed to I.K. (komuro-tky@umin.ac.jp)

Received 21 December 2007; accepted 2 April 2008; published online 20 April 2008; DOI: 10.1038/ncb1719

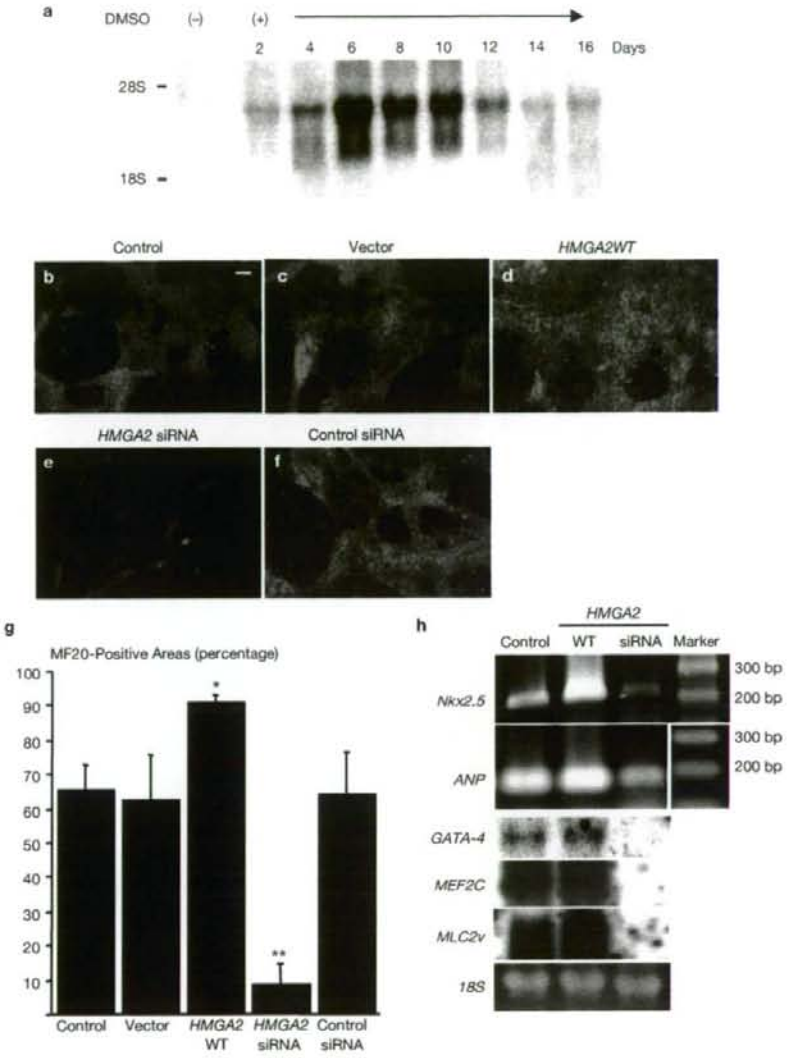

Figure 1 HMGA2 is an essential positive regulator of cardiomyocyte differentiation. (**a**) Expression of *HMGA2* mRNA during P19CL6 differentiation into cardiomyocytes was assessed by northern blot analysis. (**b–f**) The effect of *HMGA2* overexpression or *HMGA2* knockdown on cadiomyocyte differentiation was assessed with MF20 staining in control (**b**), empty vector-transfected (**c**), *HMGA2* overexpressing (**d**), *HMGA2* siRNA-transfected (**e**) and control siRNA-transfected (**f**) P19CL6 cells. Scale bar is 100 μm. (**g**) Quantification of MF20-positive area. The results are shown as mean ± s. d. $*P < 0.05$, compared with control or vector-transfected cells, $**P < 0.01$ compared with control or irrelevant siRNA-transfected cells (one-way ANOVA, followed by Fisher's PLSD test; $n = 6$) (**h**) The effect of *HMGA2* overexpression or *HMGA2* knockdown on cardiac marker gene expression was assessed by RT-PCR (for *Nkx2.5* and *atrial natriuretic peptide* (*ANP*)) and northern blot (for *GATA-4*, *MEF2C* and *myosin light chain 2v* (*MLC2v*)).

generated by alternative splicing of *HMGA1* gene transcripts, and HMGA2, encoded by the *HMGA2* gene. All HMGA proteins except HMGA1c contain three short basic repeats called AT-hooks, which bind to the minor groove of AT-rich DNA stretches[1]. HMGA proteins are also able to associate with multiple transcription factors and regulate the expression of their target genes. For example, expression of the interferon-β gene is regulated by a multiprotein complex containing NF-κB, interferon regulatory factor, activating transcription factor-2/c-Jun and HMGA1a[9]. HMGA proteins also participate in the regulation of the genes for interleukin-2 receptor α and the insulin receptor[10,11]. HMGA proteins are expressed ubiquitously and abundantly during embryogenesis, whereas their expression is low or undetectable in fully differentiated adult tissues[1,2]. This suggests that HMGA proteins regulate normal cell growth and differentiation.

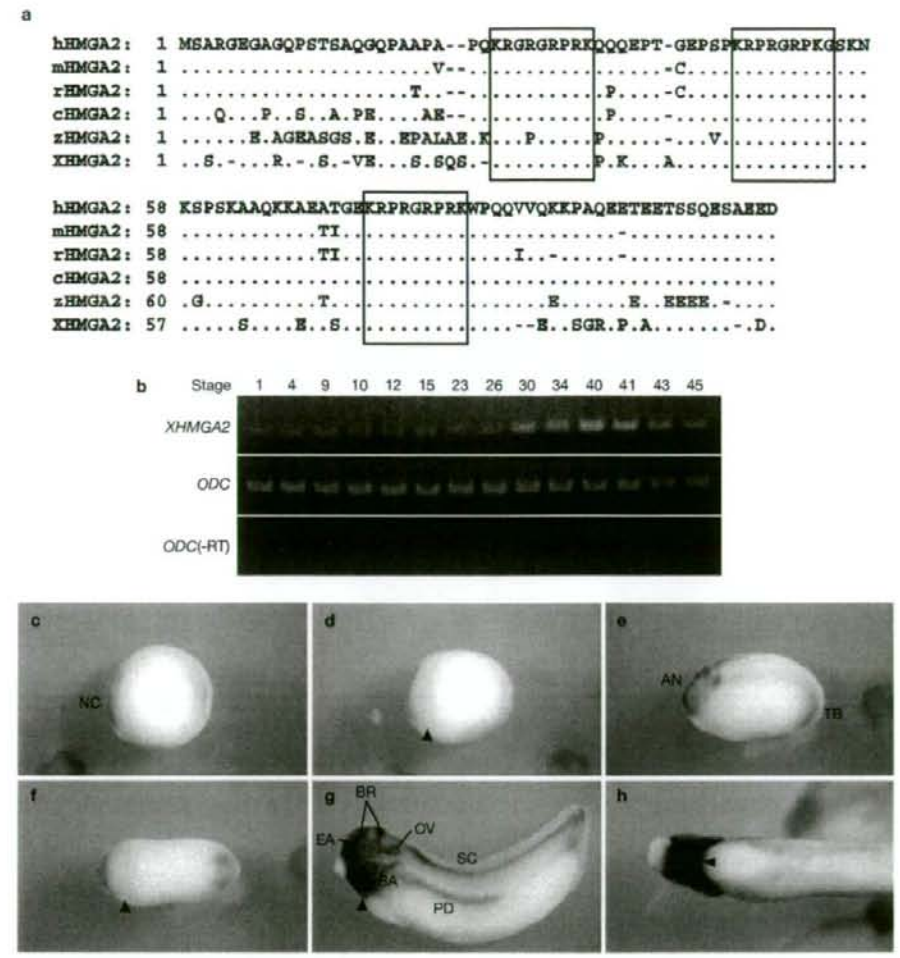

Figure 2 cDNA sequence and expression pattern of *XHMGA2*. (**a**) Amino-acid sequences of XHMGA2 protein were compared with those of human (NM_001094371), mouse (NM_010441), rat (NM_032070), chicken (NM_205001) and zebrafish (NM_212680) HMGA2. Dots indicate identities and dashed lines are introduced to maximize the alignment. Boxes represent the three AT-hooks. (**b**) Expression of *XHMGA2* mRNA during embryogenesis analysed by RT-PCR. *Ornithine decarboxylase* (*ODC*) represents internal controls. (**c–h**) Expression of *XHMGA2* mRNA during embryogenesis analysed by *in situ* hybridization. Lateral (**c**) and ventral (**d**) view of stage-15 embryo. *XHMGA2* expression was detected in neural crest (NC) and weakly in precardiac region (arrowhead). Lateral (**e**) and ventral (**f**) view of stage-23 embryo. *XHMGA2* was expressed in anterior neural tissue (AN), tailbud (TB) and weakly in precardiac region (arrowhead). Lateral (**g**) and ventral (**h**) view of stage-32 embryo. *XHMGA2* was detected in brain (BR), spinal cord (SC), eye anlage (EA), otic vesicle (OV), branchial arch (BA), pronephric duct (PD) and heart anlage (arrowhead). Anterior is left and dorsal is top for **c**, **e**, **g**, and anterior is left for **d**, **f**, **h**.

To examine whether HMGA2 regulates cardiomyocyte differentiation, we analysed the ability of P19CL6 clones stably overexpressing wild-type *HMGA2* (P19CL6–HMGA2) to differentiate into cardiomyocytes. The extent of cardiomyocyte differentiation was assessed by the area positive for an anti-α-myosin heavy chain antibody (MF20). In response to DMSO, P19CL6–HMGA2 differentiated into beating cardiomyocytes more efficiently than the parental P19CL6 cells (Fig. 1b–d, g), and there was a positive correlation between the extent of cardiomyocyte differentiation and the level of *HMGA2* expression in multiple P19CL6–HMGA2 clones (Supplementary Information, Fig. S1a). On the other hand, siRNA-mediated knockdown of *HMGA2* blocked cardiomyocyte differentiation of P19CL6 cells without altering the expression of mesodermal marker genes such as *Brachyury* and *Flk-1*, whose expressions precede those of early cardiac marker genes such as *Nkx2.5* (Fig. 1e–g; Supplementary Information, Fig. S1b). The expression levels of cardiac marker genes was upregulated in response to HMGA2 overexpression, whereas they were downregulated by knockdown of *HMGA2* expression (Fig. 1h). Together, these results suggest that HMGA2 is an essential positive regulator of cardiomyocyte differentiation.

To investigate the role of HMGA2 in cardiogenesis *in vivo*, we performed experiments using *Xenopus* embryos. We first cloned *XHMGA2*, a *Xenopus* orthologue of *HMGA2*. *XHMGA2* encodes a protein of 105

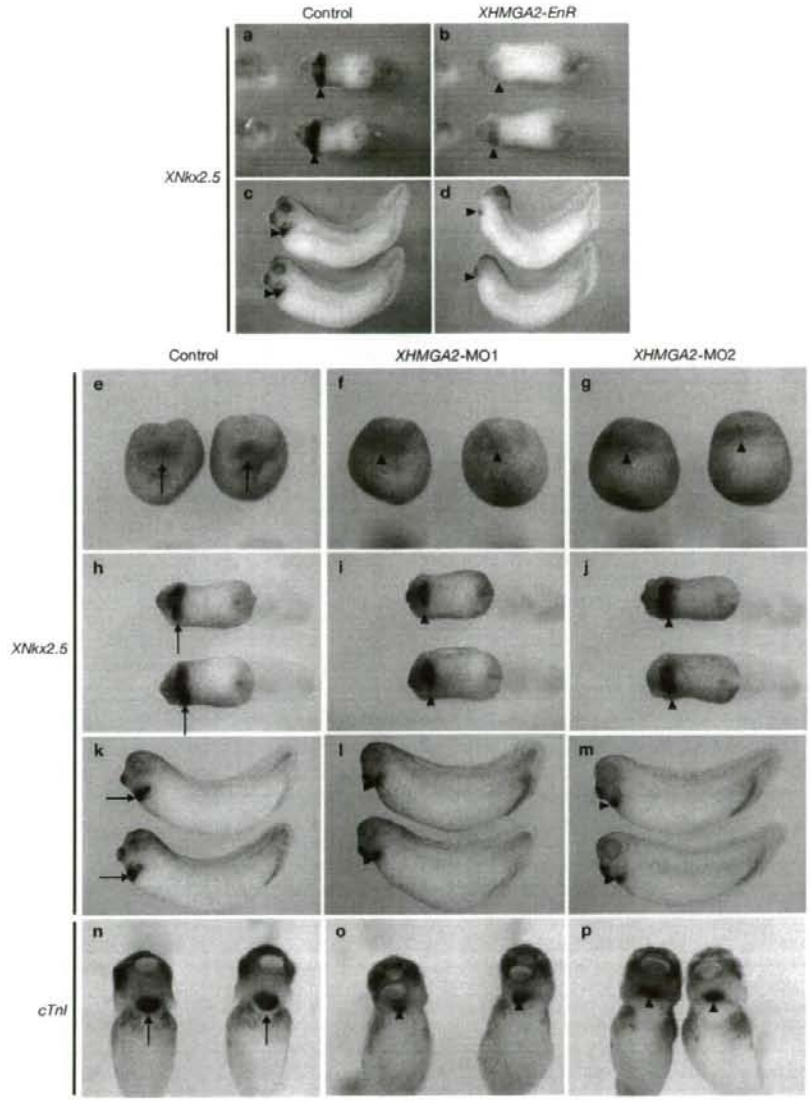

Figure 3 XHMGA2 is essential for cardiogenesis. (**a–d**) Overexpression of a dominant-negative *XHMGA2* mutant in *Xenopus* embryos blocked *XNkx2.5* expression. Ventral view of stage-23 (**a**, **b**) and lateral view of stage-34 (**c**, **d**) embryos. Expression of *XNkx2.5* mRNA was decreased in *XHMGA2–EnR* mRNA-injected embryos (**b**, **d**, arrowheads), compared with that of control embryos (**a**, **c**, arrowheads). (**e–p**) MO-mediated *XHMGA2* knockdown results in impaired cardiogenesis. Whole-mount *in situ* hybridization analysis was performed sequentially for *Xenopus* embryos at stage 15 (**e–g**), stage 23 (**h–j**) and stage 34 (**k–m**) for *XNkx2.5*, and at stage 41 for *cardiac troponin I* (*cTnI*) (**n–p**). Expression of *XNkx2.5* mRNA was detected in uninjected control embryos (**e**, **h**, **k**, arrows), whereas it was attenuated in both XHMGA2–MO1 (**f**, **i**, **l**) and XHMGA2–MO2 (**g**, **j**, **m**)-injected embryos (arrowheads). *In situ* hybridization analysis for *cardiac troponin I* revealed that the heart size in MO-injected embryos (**o**, **p**, arrowheads) was smaller than that of control embryos (**n**, arrows).

amino acids that contains three highly conserved AT-hooks and is 60–70% homologous with HMGA2 proteins in other species (Fig. 2a). Reverse transcriptase-polymerase chain reaction (RT–PCR) analysis revealed that *XHMGA2* was maternally transcribed in the early stage of embryogenesis and its expression levels increased at stage 30 (Fig. 2b). *In situ* hybridization analysis revealed that *XHMGA2* was expressed in neural crest cells and the precardiac region at the neurula stage (Fig. 2c, d), and in anterior neural tissue, tailbud and precardiac region at the early tailbud stage (Fig. 2e, f). At the late tailbud stage, a strong signal was detected in brain, spinal code, eye anlage, otic vesicle, branchial arch, pronephric duct and heart anlage (Fig. 2g, h). To examine whether XHMGA2 regulates cardiogenesis *in vivo*, we injected

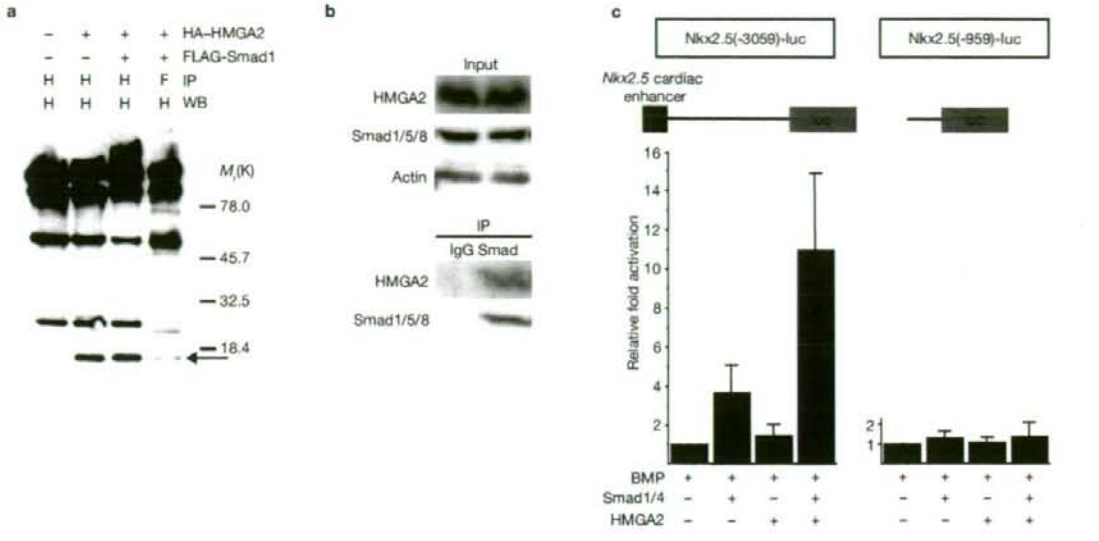

Figure 4 HMGA2 upregulates *Nkx2.5* promoter activity in collaboration with Smads. (**a**) HA–HMGA2 interacted with FLAG–Smad1 in COS7 cells, as revealed by IP-western blot (WB) analysis. HA–HMGA2 was immunoprecipitated with an anti-FLAG antibody (arrow). H, anti-HA antibody; F, anti-FLAG antibody. (**b**) Endogenous HMGA2 interacted with endogenous Smad1/5/8 in P19CL6 cells. IP-western blot analysis revealed that a positive HMGA2 signal was detected in anti-Smad1/5/8 immunoprecipitates but not in control rabbit-IgG immunoprecipitates. (**c**) Luciferase reporter gene assay using Nkx2.5(−3059)-luc and Nkx2.5(−959)-luc. HMGA2 and Smad1/4 showed synergistic transactivation of −3059 bp *Nkx2.5* promoter but not −959bp *Nkx2.5* promoter. *Nkx2.5* cardiac enhancer at −3059/−2554 is shown as a blue box. The results are expressed as mean ± s. d. ($n = 6$).

mRNA encoding a dominant-negative mutant of XHMGA2 at the 8-cell stage into the dorsal region of two dorsal-vegetal blastomeres fated to be heart and liver anlage. Dominant-negative XHMGA2 was constructed as a fusion protein of full-length XHMGA2 and a transcriptional repressor domain of *Drosophila melanogaster* engrailed (XHMGA2–EnR)[12]. *In situ* hybridization analysis revealed that the expression of *Xenopus Nkx2.5* (*XNkx2.5*) was markedly downregulated in embryos injected with *XHMGA2–EnR* mRNA (Fig. 3a–d). We also used a morpholino (MO)-mediated knockdown strategy to downregulate XHMGA2 expression. Two different non-overlapping MOs (*XHMGA2*–MO1 and *XHMGA2*–MO2), which were confirmed to specifically recognize the target sequences of *XHMGA2* mRNA (Supplementary Information, Fig. S2), were injected into the dorsal region of two dorsal-vegetal blastomeres at the 8-cell stage. *In situ* hybridization analysis showed downregulation of *XNkx2.5* expression in MO-injected embryos and this effect of *XHMGA2* knockdown was observed from the neurula stage (Fig. 3e–m). *In situ* hybridization analysis of *cardiac troponin I* at the tadpole stage showed that the hearts of MO-injected embryos were reduced in size, compared with control embryos (Fig. 3n–p), and rhythmic contraction of the heart, normally observed at this stage, was attenuated or completely absent in MO-injected embryos (Supplementary Information, Movie 1). These phenotypes of morphants were rescued by co-injection of MO-resistant *XHMGA2* plasmid DNA (Supplementary Information, Fig. S3). These results strongly suggest that HMGA2 is essential for normal cardiac development *in vivo*.

Marked upregulation of *Nkx2.5* in P19CL6 cells by HMGA2 overexpression, compared with other early cardiac-marker genes such as *GATA-4* or *MEF2C* (Fig. 1h) suggests that *Nkx2.5* may be a direct target gene of HMGA2. BMP is a potent positive regulator of *Nkx2.5* expression during cardiogenesis[13]. BMP treatment causes the formation of heterooligomers containing BMP-specific Smad1/5/8 and the common-mediator Smad4, which translocate to the nucleus and activate transcription[14]. It has been shown that conserved binding sites for Smad proteins are required for cardiac-specific *Nkx2.5* enhancer activity[15,16]. We therefore tested the hypothesis that HMGA2 mediates BMP-responsive expression of *Nkx2.5* gene in collaboration with the Smad family of transcription factors. We first examined whether HMGA2 interacts with BMP-responsive Smads. Immunoprecipitation (IP)-western blot analysis of COS7 cell lysate cotransfected with HA-tagged HMGA2 and FLAG-tagged Smad1 showed that HMGA2 and Smad1 interacted with each other (Fig. 4a). Similar IP-western analysis demonstrated that endogenous HMGA2 interacted with endogenous Smad1/5/8 in P19CL6 cells treated with DMSO for 6 days (Fig. 4b). We also tested whether HMGA2 and Smads cooperatively regulate *Nkx2.5* promoter activity. In the presence of BMP stimulation, Smad1/4, but not HMGA2, transactivated the −3059 bp murine *Nkx2.5* promoter, and simultaneous expression of Smad1/4 and HMGA2 showed synergistic promoter activation (Fig. 4c, left panel). Deletion of the promoter region between −3059 and −959 resulted in a loss of transactivation by Smad1/4 and HMGA2 (Fig. 4c, right panel). These observations suggest that HMGA2 and Smad1/4 form a protein complex and synergistically upregulate *Nkx2.5* promoter activity, and that the HMGA2/Smad-responsive element(s) is located at −3059/−959 of the *Nkx2.5* regulatory region.

Previously, a cardiac enhancer at −3059/−2554 in *Nkx2.5* 5′-flanking region was characterized[17], which contains four Smad binding elements (SBEs) at −3038 (SBE-1), −3027 (SBE-2), −2774 (SBE-3) and −2758 (SBE-4; refs 15, 16). These SBEs are highly conserved among chick, mouse and human, and SBE-3 and SBE-4 are also conserved

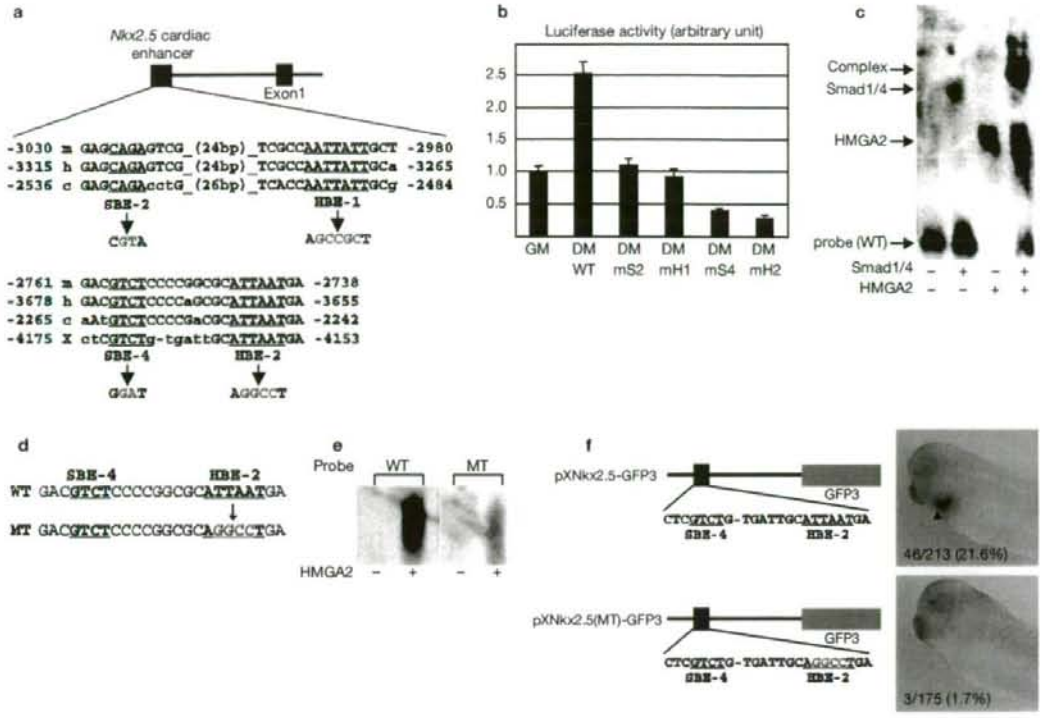

Figure 5 HMGA2 binding is required for full activation of *Nkx2.5* promoter. (**a**) Sequence comparison of SBE-2/HBE-1 and SBE-4/HBE-2 elements in the -3059/-2554 *Nkx2.5* cardiac enhancer. These elements are evolutionarily conserved in human, mouse and chick, and SBE-4/HBE-2 sites are also conserved in *Xenopus*. Nucleotides that are not conserved are shown by small letters: m, mouse; h, human; c, chick; x, *Xenopus*. (**b**) Mutations introduced into conserved SBE-2/HBE-1 and SBE-4/HBE-2 elements attenuated *Nkx2.5* promoter activity during cardiomyocyte differentiation of P19CL6 cells. *Nkx2.5* promoter activity was assessed in P19CL6 cells at day 6 of differentiation. GM, growth medium (without DMSO); DM, differentiation medium (containing 1% DMSO); WT, wild-type *Nkx2.5* promoter; mS2, mH1, mS4 and mH2, *Nkx2.5* promoter containing mutations at SBE-2, HBE-1, SBE-4 and HBE-2, respectively ($n = 3$). (**c**) Interaction between Smad1/4 and HMGA2 on the SBE-4/HBE-2 element, as revealed by EMSA. Smad1/4 and HMGA2, either alone or in combination, bound to a 24-bp probe containing the SBE-4/HBE-2 element. (**d**) Sequences used for the EMSA probe. Mutations introduced into the HBE-2 site are shown in red. WT, wild-type probe; MT, mutated probe. (**e**) Binding of HMGA2 to SBE-4/HBE-2 element was reduced by mutations introduced into the HBE-2 site. (**f**) *GFP* reporter genes used to generate transgenic *Xenopus* embryos are shown on the left. pXNkx2.5(mt)-GFP plasmid contains mutations in the conserved HBE-2 site, which are indicated by red. GFP expression as assessed by *in situ* hybridization is shown on the right panels. The number of embryos showing *GFP* expression (arrowhead) per total number of surviving embryos for both plasmids are indicated.

in *Xenopus*[18], suggesting that this cardiac enhancer may be a target of HMGA2 and Smads. Indeed, there were two potential AT-rich HMGA2 binding elements (HBEs) adjacent to SBE-2 and SBE-4 (Fig. 5a). These HBEs were conserved in chick, mouse and human, and HBE-2 was also conserved in *Xenopus*[15,16,18]. Mutations introduced into SBE-2 or HBE-1 reduced the promoter activity of *Nkx2.5* by 50–60%, and more than 80% reduction in the promoter activity was observed by mutations introduced into SBE-4 or HBE-2 (Fig. 5b), suggesting that HMGA2 and Smads regulate *Nkx2.5* promoter activity cooperatively through these elements. As mutations introduced into the proximal element containing SBE-4/HBE-2 had a profound effect on *Nkx2.5* promoter activity, a 24-bp sequence containing SBE-4/HBE-2 (Fig. 5a, d) was used as a probe to examine protein–DNA interactions. Electrophoretic mobility shift assay (EMSA) showed that Smad1/4, HMGA2 and a complex containing Smad1/4 and HMGA2 bound to the 24-bp sequence (Fig. 5c). Mutation of the A/T-rich HBE-2 markedly attenuated the ability of HMGA2 to bind to this sequence (Fig. 5d, e). We also analysed *XNkx2.5* promoter activity *in vivo* in transgenic *Xenopus* embryos. Transgenic embryos expressing *green fluorescent protein* (*GFP*) gene under the control of the –4295 bp *XNkx2.5* promoter, which contains conserved SBE-4 and HBE-2, were assayed for their *GFP* mRNA expression by *in situ* hybridization. The *GFP* transgene containing the –4295 bp *XNkx2.5* promoter induced detectable *GFP* expression in the heart, and mutations introduced into HBE-2 abolished it (Fig. 5f). These findings suggest that HMGA2 and BMP-responsive Smads upregulate *Nkx2.5* promoter activity cooperatively through Smad- and HMGA2-binding elements, and that the conserved HMGA2 binding site is essential for *Nkx2.5* expression both *in vitro* and *in vivo*.

In this study we have demonstrated that HMGA2 promotes cardiomyocyte differentiation *in vitro* and is essential for cardiogenesis both *in vitro* and *in vivo*. Expression of HMGA2 is high during embryogenesis but low or undetectable in the adult tissues, suggesting that HMGA2 regulates normal cell growth and differentiation in general. Of note, transient expression of HMGA2 was observed in the heart after myocardial

infarction (Supplementary Information, Fig. S4), suggesting that HMGA2 is one of the fetal genes re-expressed in the myocardium in response to biomechanical stress. HMGA2 has been implicated in both benign and malignant tumours. Rearrangement of *HMGA2*, which results in the generation of a chimaeric or a truncated HMGA2 protein that contains three AT-hooks but lacks its carboxy-terminus, is frequently observed in benign human tumours of mesenchymal origin[19]. Overexpression of wild-type HMGA2 has also been reported in several malignant tumours[19]. Moreover, transgenic mice overexpressing the C-terminal-truncated form of HMGA2 are large and obese with lipomas[20,21]. Targeted disruption of the *HMGA2* gene in mice causes general growth retardation and impaired adipocyte differentiation[22,23], consistent with the suggestion that HMGA2 regulates cell growth and differentiation. In the experiments shown in Fig. 3, MOs were injected into the dorsal region of two dorsal-vegetal blastomeres fated to be heart and liver anlage. Examination of other lineage markers under these experimental conditions revealed that the expression of *XHex*, a marker gene for liver and thyroid gland, was attenuated in the liver and absent in the thyroid gland (Supplementary Information, Fig. S5d–f). Similarly, *Xmsr*, an endothelial-cell marker gene, showed a perturbed pattern of expression (Supplementary Information, Fig. S5g–i). Furthermore, when *XHMGA2*-MOs were injected into other regions at the 8-cell stage (Supplementary Information, Fig. S6a), different phenotypes of morphants were observed, depending on the site of MO injection and the area of MO distribution (Supplementary Information, Fig. S6b–f). Thus, the phenotype of *XHMGA2* knockdown is not necessarily restricted to the heart.

In this study we have also demonstrated that HMGA2 forms a protein complex with BMP-responsive Smad transcription factors that coordinately upregulate the promoter activity of *Nkx2.5* through evolutionarily conserved Smad- and HMGA2-binding elements. As HMGA2 has been shown to regulate the proliferation and/or differentiation of multiple cell types, there is a possibility that the regulation of cardiogenesis by HMGA2 is indirect and mediated by its effects on other cell types. However, we favour the idea that HMGA2 regulates cardiomyocyte differentiation directly, as our data suggest that HMGA2 promotes cardiogenesis through the transcriptional activation of *Nkx2.5*. Specifically, reduced expression of *Nkx2.5* by inhibition of HMGA2 and downregulation of *Nkx2.5* promoter activity by mutations in the HBE-2 site both *in vitro* and *in vivo* strongly suggest that *Nkx2.5* is a direct target of HMGA2. In this regard it is noteworthy that HMGA2 regulates the expression of an organ-specific transcription factor in collaboration with a growth factor-mediated signalling system and consequently contributes to organogenesis. In contrast to the *Nkx2.5* promoter, there was no cooperative upregulation of the BMP-responsive reporter BRE-luc or the TGF-β-responsive reporter p3TP-luc by the co-expression of Smad1/4/HMGA2 or Smad2/4/HMGA2, (Supplementary Information, Fig. S7). Thus, HMGA2 is not generally involved in transcriptional regulation mediated by Smads, but rather, is required for a specific subset of Smad-responsive transcriptional regulation in a context-dependent manner. Simultaneous interaction of HMGA2 with DNA and Smads with DNA may be necessary for synergistic transactivation by HMGA2 and Smads.

We speculate that the defect in cardiogenesis induced by HMGA2 inactivation is caused by downregulation of BMP-mediated *Nkx2.5*, as inactivation of *Nkx2.5* is sufficient to disrupt normal heart formation *in vivo*[4]. However, the possibility that HMGA2 is required for the proliferation of embryonic cardiomyocytes cannot be excluded. *HMGA2* knockdown in *Xenopus* embryos resulted in cardiac defects, whereas no cardiac abnormalities have been reported in *HMGA2* knockout mice. Although the exact reason for this apparent discrepancy is not clear at this time, the lack of cardiac phenotype in *HMGA2* mutant mice may be due to the genetic redundancies between *HMGA1* and *HMGA2* or among other HMG family members. As HMGA2 seems to regulate the early stage of cardiac development, further studies on this molecule may provide insights into myocardial regenerative medicine and the pathophysiology of congenital heart diseases. □

METHODS

Plasmids and reagents. pcDNA3–HMGA2 was provided by G. Manfioletti (University of Trieste, Italy). FLAG-tagged Smad1/2/4, GST–Smad1/4 and p3TP-luc have been described previously[24]. BRE-luc was provided by P. ten Dijke (Leiden University Medical Center, Netherlands)[25]. Nkx2.5(−3059)-luc and Nkx2.5(−959)-luc were provided by K. E. Yutzey (Cincinnati Children's Medical Center, Cincinnati, OH)[15]. pCS-Fast-EnR was provided by M. Whitman (Harvard Medical School, Boston, MA)[12]. XCarGFP3 was provided by E. Amaya (University of Manchester, UK)[26]. Natural bovine BMP cocktail was purchased from Sangi.

Differential mRNA display. Differential mRNA display and subcloning of re-amplified cDNA fragments were performed as described previously[27].

P19CL6 cell culture and stable transformants. P19CL6 cells were cultured and induced to differentiate into cardiomyocytes as described previously[8]. To obtain P19CL6 clones stably overexpressing *HMGA2*, pcDNA3–HMGA2 was transfected into P19CL6 cells and neomycin-resistant clones were selected.

siRNA-mediated knockdown in P19CL6 cells. For *HMGA2* knockdown, 2-For-Silencing siRNA kit (Qiagen) was used. siRNAs were transfected at day 2 of differentiation. Sequences of *HMGA2* siRNA were as follows. Duplex 1: r(AGU AUA AGU UAA UAC UGA A)dTdT for sense, r(UUC AGU AUU AAC UUA UAC U)dGdA for antisense. Duplex 2: r(GGA AAU CUA CAC AGC CAA A)dTdT for sense, r(UUU GGC UGU GUA GAU UUC C)dCdG for antisense. MARK1 siRNA included in the kit was used as an irrelevant control siRNA.

Immunocytochemisry. Immunostaining with an anti-MF20 antibody was performed as described previously[8]. MF20-positive areas were measured at day 14 of differentiation.

RNA analysis. Northern blot, RT-PCR and quantitative real-time PCR for RNA analysis in P19CL6 cells were performed as described previously[8,28]. In *Xenopus* embryos, RT-PCR was performed as described previously[29]. PCR primers and PCR conditions are available in the Supplementary Information.

IP-western blot analysis. Total cell lysate was prepared from COS7 cells transfected with expression vectors for HA–HMGA2 and FLAG–Smad1 from P19CL6 cells induced to differentiate for 6 days. IP-western blot analysis was performed essentially as described previoulsy[30] using anti-HA monoclonal antibody 12CA5 (Roche) and anti-FLAG monoclonal antibody M2 (Kodak) for COS7 cell lysate, and anti-Smad1/5/8 and anti-HMGA2 (HMGI-C) rabbit polyclonal antibodies (Santa Cruz) for P19CL6 cell lysate.

Luciferase reporter gene assay. Nkx2.5–luc, pRL–CMV (an internal control) and effector constructs were transfected into COS7 cells or P19CL6 cells, and luciferase activity was measured with a luminometer (Berthold Lumat LB9507) 48 h after transfection. BMP cocktail (100 ng ml^{-1}) was added to COS7 medium. Mutations were introduced into Nkx2.5–luc plasmid using QuikChange II Site-Directed Mutagenesis Kit (Stratagene).

EMSA. Probes for EMSA were labelled using Biotin 3′ End DNA Labeling Kit (Pierce Biotechnology) and EMSA was performed using the LightShift Chemiluminescent EMSA Kit (Pierce Biotechnology). The HMGA2 protein

(HMGIC(48–109)-NH_2) was purchased from Phoenix Pharmaceuticals. GST–Smad1 and GST–Smad4 fusion proteins were purified with B-PER GST Spin Purification Kit (Pierce Biotechnology).

Isolation of *XHMGA2* cDNA. The entire coding region of *XHMGA2* was amplified by RT-PCR using mRNA obtained from embryos at the early tailbud stage, based on the sequence of a *Xenopus* EST (NM_001094371), which encodes a full-length protein similar to human HMGA2. The following primers were used: XHMGA2-U (5′-ATG AGC TCA AGG GAA GGA GCC-3′), XHMGA2-D (5′-CTA GTC GTC TTC AGA TTC CTG GG-3′). We cloned the PCR product into a pCS2+ vector (pCS2+XHMGA2).

Microinjection of *XHMGA2–EnR* mRNA. An expression vector for *XHMGA2–EnR* was constructed by a PCR-based cloning strategy. A cDNA fragment encoding Engrailed repressor domain (EnR) was amplified from *FAST–EnR* plasmid by PCR. mRNA for microinjection was synthesized with mMESSAGE mMACHINE kit (Ambion) from plasmids encoding *XHMGA2–EnR*. Synthesized mRNAs were microinjected as described previously[29].

MO experiments. The sequences of *XHMGA2* MOs were: *XHMGA2*–MO1, 5′-AGC TCA TGG TAG AGA GTG TGT GTG C-3′; XHMGA2-MO2, 5′-GCC CGG CGA TCC TGG AGC ACC TTA A-3′. MO activities and specificities were checked by co-injection of *5′XHMGA2–EGFP* or *XHMGA2–EGFP* mRNA (Supplementary Information, Fig. S2). For this, the *XHMGA2* coding region with 73 bp 5′ untranslated region (UTR) and *XHMGA2* coding region without 5′UTR (Supplementary Information, Fig. S2a) were inserted into the *Cla*I site of the EGFP–CS2 vector[29] to construct expression vectors for 5′XHMGA2–EGFP and XHMGA2–EGFP, respectively. We injected the MOs into two dorsal-vegetal blastomeres at the 8-cell stage. Rescue experiments were performed by injecting optimal-effect doses of XHMGA2–MO1 or XHMGA2–MO2 in conjunction with pCS2+*XHMGA2* plasmid DNA, which lacks 5′UTR and therefore is MO-resistant (100 pg per embryo). For tracing of injected MOs, β-*gal* mRNA was co-injected and embryos were pre-stained with Red-gal (Research Organics) before whole-mount *in situ* hybridization.

Whole-mount *in situ* hybridization. The following plasmid templates were linearized, and digoxigenin-substituted antisense RNA probes were transcribed with T7 or SP6 RNA polymerase: *XNkx2.5, XHex, Xmsr* and *XHMGA2* (a PCR-amplified coding region subcloned into pBluescript II SK+); *Xenopus cardiac troponin I* (a PCR amplified coding region subcloned into pGEM-T Easy). Embryos were processed for whole-mount *in situ* hybridization using BM purple substrate (Roche) and then the processed pigmented embryos were bleached by 9% H_2O_2, 21% H_2O and 70% methanol.

Generation and analysis of transgenic *Xenopus* embryos. pXNkx2.5–GFP3 was generated by replacing the *cardiac actin* promoter in XCarGFP3 (ref. 18) with 4295 bp promoter sequence of *XNkx2.5*. This fragment was amplified by PCR from *Xenopus* tailbud genomic DNA using the XNkx2.5p-U primer (5′-ACC TGA GCT CGG GGG GAA TAT ACA CAA GGC C-3′) and XNkx2.5p-D primer (5′-GCA CCG GTG ACG GTA TCA GGT AAA CCC CAC A-3′). pXNkx2.5(mt)–GFP3 was created by site-directed mutagenesis. Both plasmids were digested by *Sac*I and injected. Generation of transgenic *Xenopus* embryos was carried out as described previously[31].

Accession codes. USCD-Nature Signaling Gateway (**http://www.signaling-gateway.org**): **A001667, A001029** and **A001503**

Note: Supplementary Information is available on the Nature Cell Biology website.

ACKNOWLEDGEMENTS

We thank G. Manfioletti, P ten Dijke, K. E. Yutzey, M. Whitman and E. Amaya for providing plasmids, and C. Masuo and Y. Itoh for their excellent technical assistance. This work was supported by grants from the Ministry of Education, Culture, Sports, Science and Technology, and Health and Labor Sciences Research Grants; an Academic Award of the Mochida Memorial Foundation and Uehara Memorial Foundation (to I. K.); and a Grant-in-Aid for Scientific Research from the Ministry of Education, Culture, Sports, Science and Technology of Japan (to K. M.).

AUTHOR CONTRIBUTIONS

K. Monzen, Y. I. and A. T. M. contributed equally to this work; I. K. designed and supervised the research; K. Monzen, Y. I., A. T. M., H. K., Y. H. and D. H. performed experiments; I. S., T. Y., K. Miyazono, M. A. and R. N. contributed new reagents/analytical tools; K. Monzen, Y. I. and A. T. M. analysed the data; K. Monzen, Y. I., I. S. and I. K. prepared the manuscript.

COMPETING FINANCIAL INTERESTS

The authors declare no competing financial interests.

Published online at http://www.nature.com/naturecellbiology/
Reprints and permissions information is available online at http://npg.nature.com/reprintsandpermissions/

1. Reeves, R. Molecular biology of HMGA proteins: hubs of nuclear function. *Gene* **277,** 63–81 (2001).
2. Sgarra, R. *et al.* Nuclear phosphoproteins HMGA and their relationship with chromatin structure and cancer. *FEBS Lett.* **574,** 1–8 (2004).
3. Hock, R., Furusawa, T., Ueda, T. & Bustin, M. HMG chromosomal proteins in development and disease. *Trends Cell. Biol.* **17,** 72–79 (2007).
4. Srivastava, D. Genetic assembly of the heart: implications for congenital heart disease. *Annu. Rev. Physiol.* **63,** 451–469 (2001).
5. Olson, E. N. & Schneider, M. D. Sizing up the heart: development redux in disease. *Genes Dev.* **17,** 1937–1956 (2003).
6. Hoffman, J. I. & Kaplan, S. The incidence of congenital heart disease. *J. Am. Coll. Cardiol.* **39,** 1890–1900 (2002).
7. Foley, A. & Mercola, M. Heart induction: embryology to cardiomyocyte regeneration. *Trends Cardiovasc. Med.* **14,** 121–125 (2004).
8. Monzen, K. *et al.* Bone morphogenetic proteins induce cardiomyocyte differentiation through the mitogen-activated protein kinase kinase kinase TAK1 and cardiac transcription factors Csx/Nkx-2.5 and GATA-4. *Mol. Cell. Biol.* **19,** 7096–105 (1999).
9. Yie, J., Merika, M., Munshi, N., Chen, G. & Thanos, D. The role of HMG I(Y) in the assembly and function of the IFN-β enhanceosome. *EMBO J.* **18,** 3074–3089 (1999).
10. Reeves, R., Leonard, W. J. & Nissen, M. S. Binding of HMG-I(Y) imparts architectural specificity to a positioned nucleosome on the promoter of the human interleukin-2 receptor α gene. *Mol. Cell. Biol.* **20,** 4666–4679 (2000).
11. Brunetti, A., Manfioletti, G., Chiefari, E., Goldfine, I. D. & Foti, D. Transcriptional regulation of human insulin receptor gene by the high-mobility group protein HMGI(Y). *FASEB J.* **15,** 492–500 (2001).
12. Watanabe, M. & Whitman, M. FAST-1 is a key maternal effector of mesoderm inducers in the early *Xenopus* embryo. *Development* **126,** 5621–5634 (1999).
13. Schultheiss, T. M., Burch, J. B. & Lassar, A. B. A role for bone morphogenetic proteins in the induction of cardiac myogenesis. *Genes Dev.* **11,** 451–462 (1997).
14. Heldin, C. H., Miyazono, K. & ten Dijke, P. TGFβ signalling from cell membrane to nucleus through SMAD proteins. *Nature* **390,** 465–471 (1997).
15. Liberatore, C. M., Searcy-Schrick, R. D., Vincent, E. B. & Yutzey, K. E. *Nkx-2.5* gene induction in mice is mediated by a Smad consensus regulatory region. *Dev. Biol.* **244,** 243–256 (2002).
16. Lien, C. L., McAnally, J., Richardson, J. A. & Olson, E. N. Cardiac-specific activity of an Nkx2-5 enhancer requires an evolutionarily conserved Smad binding site. *Dev. Biol.* **244,** 257–266 (2002).
17. Schwartz, R. J. & Olson, E. N. Building the heart piece by piece: modularity of *cis*-elements regulating Nkx2-5 transcription. *Development* **126,** 4187–4192 (1999).
18. Sparrow, D. B. *et al.* Regulation of the tinman homologues in *Xenopus* embryos. *Dev. Biol.* **227,** 65–79 (2000).
19. Fusco, A. & Fedele, M. Roles of HMGA proteins in cancer. *Nature Rev. Cancer* **7,** 899–910 (2007).
20. Battista, S. *et al.* The expression of a truncated HMGI-C gene induces gigantism associated with lipomatosis. *Cancer Res.* **59,** 4793–4797 (1999).
21. Arlotta, P. *et al.* Transgenic mice expressing a truncated form of the high mobility group I-C protein develop adiposity and an abnormally high prevalence of lipomas. *J. Biol. Chem.* **275,** 14394–14400 (2000).
22. Zhou, X., Benson, K. F., Ashar, H. R. & Chada, K. Mutation responsible for the mouse pygmy phenotype in the developmentally regulated factor HMGI-C. *Nature* **376,** 771–774 (1995).
23. Anand, A. & Chada, K. *In vivo* modulation of Hmgic reduces obesity. *Nature Genet.* **24,** 377–380 (2000).
24. Imamura, T. *et al.* Smad6 inhibits signalling by the TGF-β superfamily. *Nature* **389,** 622–626 (1997).
25. Korchynskyi, O. & ten Dijke, P. Identification and functional characterization of distinct critically important bone morphogenetic protein-specific response elements in the Id1 promoter. *J. Biol. Chem.* **277,** 4883–4891 (2002).
26. Brackenridge, R. A., Mohun, T. J. & Amaya, E. A role for BMP signalling in heart looping morphogenesis in *Xenopus*. *Dev. Biol.* **232,** 191–203 (2001).
27. Hosoda, T. *et al.* A novel myocyte-specific gene *Midori* promotes the differentiation of P19CL6 cells into cardiomyocytes. *J. Biol. Chem.* **276,** 35978–35989 (2001).
28. Naito, A. T. *et al.* Developmental stage-specific biphasic roles of Wnt/β-catenin signaling in cardiomyogenesis and hematopoiesis. *Proc. Natl Acad. Sci. USA* **103,** 19812–19817 (2006).
29. Michiue, T. *et al.* Xldax, an inhibitor of the canonical Wnt pathway, is required for anterior neural structure formation in *Xenopus*. *Dev. Dyn.* **230,** 79–90 (2004).
30. Hiroi, Y. *et al.* Tbx5 associates with Nkx2-5 and synergistically promotes cardiomyocyte differentiation. *Nature Genet.* **28,** 276–280 (2001).
31. Kroll, K. L. & Amaya, E. Transgenic *Xenopus* embryos from sperm nuclear transplantations reveal FGF signaling requirements during gastrulation. *Development* **122,** 3173–3183 (1996).

THE JOURNAL OF BIOLOGICAL CHEMISTRY VOL. 284, NO. 12, pp. 7832–7842, March 20, 2009

mTORC1 Activation Regulates β-Cell Mass and Proliferation by Modulation of Cyclin D2 Synthesis and Stability*[S]

Received for publication, September 25, 2008, and in revised form, December 29, 2008 Published, JBC Papers in Press, January 14, 2009, DOI 10.1074/jbc.M807458200

Norman Balcazar[‡], Aruna Sathyamurthy[‡], Lynda Elghazi[‡], Aaron Gould[‡], Aaron Weiss[‡], Ichiro Shiojima[§], Kenneth Walsh[§], and Ernesto Bernal-Mizrachi[‡1]

From the [‡]Washington University School of Medicine, Division of Endocrinology, Metabolism & Lipid Research, St. Louis, Missouri, 63110 and the [§]Boston University Medical School, Molecular Cardiology/Whitaker Cardiovascular Institute, Boston, Massachusetts 02118

Growth factors, insulin signaling, and nutrients are important regulators of β-cell mass and function. The events linking these signals to the regulation of β-cell mass are not completely understood. The mTOR pathway integrates signals from growth factors and nutrients. Here, we evaluated the role of the mTOR/raptor (mTORC1) signaling in proliferative conditions induced by controlled activation of Akt signaling. These experiments show that the mTORC1 is a major regulator of β-cell cycle progression by modulation of cyclin D2, D3, and Cdk4 activity. The regulation of cell cycle progression by mTORC1 signaling resulted from modulation of the synthesis and stability of cyclin D2, a critical regulator of β-cell cycle, proliferation, and mass. These studies provide novel insights into the regulation of cell cycle by the mTORC1, provide a mechanism for the antiproliferative effects of rapamycin, and imply that the use of rapamycin could negatively impact the success of islet transplantation and the adaptation of β-cells to insulin resistance.

The defects that result in diabetes are diverse, but the loss of pancreatic β-cell mass is a critical determinant for the development of this disease (1, 2). The capacity for β-cells to expand in response to insulin resistance is required to maintain glucose homeostasis and prevent type 2 diabetes. Pancreatic β-cell mass is regulated by a dynamic balance of neogenesis, proliferation, hypertrophy, and apoptosis (3). In particular, β-cell proliferation (determined by the number of mature β-cells entering the cell cycle) has a major role in the maintenance of β-cell mass in adult life and after proliferative stimuli (4). Although there has been much research showing the role of β-cell mass in diabetes, there is a lack of knowledge pertaining to how β-cells enter the cell cycle, proliferate, and increase mass.

In pancreatic β-cells, glucose, amino acids, and growth factors have been shown to induce G_1-S progression (5–7). Recent studies have demonstrated that mTOR integrates growth factors and nutrient signals and is essential for cell growth and proliferation (8). One of the major mechanisms by which nutrient and growth factors regulate mTOR activity involves the tuberous sclerosis complex 2 (TSC2)[2] gene product (tuberin) as well as TSC1 (hamartin) and the small G protein Ras homolog enriched in brain. Phosphorylation of TSC2 by the serine-threonine kinase AKT induces mTOR signaling by derepressing the TSC2 GTPase-activating protein activity toward Ras homolog enriched in brain, (9–13). Recent findings indicate that mTOR is a part of two distinct complexes: mTORC1 and mTORC2 (14, 15). The mammalian mTORC1 contains Raptor and the G protein β-subunit-like protein (GβL). mTORC1 activates key regulators of protein translation; ribosomal S6 kinase (S6K), eukaryote initiation factor 4E-binding protein 1, and eukaryote initiation factor 4E (16). The mTORC2 complex includes mTOR and rictor and is insensitive to rapamycin (14, 15). This complex is potentially important for the regulation of β-cell mass and function, because it is responsible for the phosphorylation/activation of Akt on Ser^{473} (17). Evidence for the importance of mTOR signaling on the modulation of β-cell mass and proliferation *in vivo* comes from genetically modified mice. Decreased β-cell mass and hyperglycemia in mice deficient for S6K and mutant for ribosomal protein S6 provide evidence for the importance of this pathway in these processes (18–20). Moreover, activation of mTOR signaling by conditional deletion of TSC2 in β-cells induces β-cell proliferation and hypertrophy (21, 22) The contribution and potential role for mTOR signaling and the mTORC complexes in β-cell mass and function have yet to be adequately explored.

The current experiments delineate some of the molecular mechanisms involved in β-cell G_1-S transition by the mTOR arm of Akt signaling. In these studies, the hypothesis that the mTORC1 (mTOR/Raptor) is a major regulator of β-cell cycle progression and mass *in vivo* was tested. To test this hypothesis, we studied the effects of inhibition of the mTORC1 complex under proliferative conditions induced by controlled activation of Akt signaling in β-cells. To activate Akt signaling in a controlled fashion, we developed a doxycycline (dox)-inducible mouse model. This animal model allowed us to induce β-cell

* This work was supported, in whole or in part, by National Institutes of Health Grant R01DK073716-01 (to E. B.-M.). This work was also supported by a Career Development Award from the American Diabetes Association (to E. B.-M.). The costs of publication of this article were defrayed in part by the payment of page charges. This article must therefore be hereby marked "*advertisement*" in accordance with 18 U.S.C. Section 1734 solely to indicate this fact.

[S] The on-line version of this article (available at http://www.jbc.org) contains supplemental Fig. S1–S4.

[1] To whom correspondence should be addressed: Washington University School of Medicine, 660 S. Euclid Ave., Campus Box 8127, St. Louis, MO 63110. Tel.: 314-362-7693; Fax: 314-747-2692; E-mail: ebernal@wustl.edu.

[2] The abbreviations used are: TSC, tuberous sclerosis complex; S6K, ribosomal S6 kinase; dox, doxycycline; Cdk, cyclin-dependent kinase; DT, double transgenic; ST, single transgenic; GST, glutathione *S*-transferase; GFP, green fluorescent protein; CHAPS, 3-[(3-cholamidopropyl)dimethylammonio]-1-propanesulfonic acid; Rap, rapamycin.

proliferation and mass without disturbing peripheral tissues. These studies showed that the mTORC1 complex mediates the regulation of cell cycle in β-cells *in vivo* and does so by activation of cyclin-dependent kinase-4 (Cdk4). The regulation of cell cycle progression by mTORC1 signaling resulted from modulation of the synthesis and stability of cyclin D2, a critical regulator of β-cell cycle, proliferation, and mass. These studies indicate that the mTORC1 is major component relating proliferative signals induced by nutrients and growth factors and uncover the molecular mechanisms implicated in the regulation of β-cell cycle by this signaling pathway.

EXPERIMENTAL PROCEDURES

Mice—RIP-rtTA mice express the reverse tetracycline transactivator under the control of the rat insulin II gene and are in C57Bl/6 (B6)/CBA background (23). The tetOAkt1 mice have been previously described (24) and contain the myristoylated AKT 1 gene under the regulation of tetracycline-responsive element. Generation and phenotypic characterization of myr-Akt mice have been previously described elsewhere in detail (24). Double transgenic RIP-rtTA/tetOAkt1 mice (DT) were obtained by crossing RIP-rtTA with tetOAkt1. The single transgenic (ST) was used as control and included RIP-rtTA mice. Experiments were performed in 2-month-old males. Control and experimental animals were on comparably mixed background. Doxycycline treatment was performed by adding 2 mg/ml doxycycline to the drinking water. Mice overexpressing a constitutively active form of Akt under the control of the rat insulin promoter (*caAkt*^{RIP}) have been previously described (25). All of the procedures were performed in accordance with the Washington University Animal Studies Committee.

Islet and MIN6 Cell Culture—MIN6 cells were stably infected with a lentivirus containing a constitutively active Akt mutant (MIN6-caAkt) or GFP (MIN6-GFP) as control. These lines were maintained as described previously (26). For experiments with rapamycin, MIN6 cells were cultured with rapamycin for 16 h. The *in vitro* experiments in islets were performed in islets from ST or DT mice treated with vehicle or dox in the drinking water for 3 weeks. After isolation, the islets were cultured in medium with vehicle (ST) or dox (DT) for 40 h. Rapamycin (50 nM) or vehicle was added to the medium for the last 16 h of culture before harvesting. This experimental protocol reproducibly inhibit mTORC1 complex *in vitro*. These experimental conditions were used for all of the islet experiments except for the studies in Fig. 2*C*.

Islet Isolation and Western Blot Analysis—Islet isolation was accomplished by collagenase digestion as described previously (25). The following morning after isolation, the islets were hand picked and treated with 2 μg/μl doxycycline and/or 50 nM rapamycin for 16 h as indicated in the figures and results. Isolated islets were lysed in a buffer containing 0.3% CHAPS, 150 mM NaCl, 5 mM EDTA, 10 mM Tris, pH 8.0, and protease and phosphatase inhibitors (Roche Applied Science). Islet lysates were subjected to immunoblotting using the following antibodies: Akt, pGSK3 α/β, p70S6K (phospho-p70 S6K Thr 389) phospho-S6 ribosomal protein (Ser$^{235/236}$), cyclin D1, cyclin D3, and p27 were from Cell Signaling (Beverly, MA), and cyclin D2 was obtained from Lab Vision Corporation (Fremont, CA). Cdk4 was from Santa Cruz Biotechnology (Santa Cruz, CA), and α-tubulin was from Sigma. Secondary horseradish peroxidase-conjugated anti-rabbit and anti-mouse IgG were from Cell Signaling.

Immunohistochemistry, Islet Morphometry, and Analysis of Proliferation and Apoptosis—Pancreatic tissue was fixed overnight in 3.7% formalin solution and embedded in paraffin using standard techniques. Immunostaining for insulin was done as describe previously (25). Immunofluorescence for phospho-pS6 ribosomal protein (Ser$^{235/236}$) (Cell Signaling) and insulin was performed as described previously (25). Assessment of β-cell mass was performed by point counting morphometry from five insulin-stained sections (4 μm) separated by 200-μm National Institutes of Health ImageJ software (v1.3.8x) as described previously (27, 28). Proliferation was performed in insulin-and Ki67-stained sections (Novocastra, Burlingame, CA) from ST and DT mice. Proliferating cells were identified by co-staining for Ki67 and insulin. Apoptosis was determined in pancreatic sections stained for insulin and cleaved-caspase 3 (Cell Signaling). Co-staining for insulin and cleaved-caspase 3 identified apoptotic cells. At least 1000 insulin-stained cells were counted for each animal.

Quantitative Reverse Transcription-PCR—Total RNA was isolated using RNeasy (Qiagen). cDNA was synthesized using random hexamers and reverse transcribed with Superscript II (Invitrogen) according to the manufacturer's protocol. Real time PCR was performed on ABI 7000 sequence detection system using TaqMan gene expression assays (Applied Biosystem, Foster City, CA). Primers from cell cycle components were purchased from Applied Biosystem with reference numbers p21 (Mn 00432448), p27 (Mm 00432359), Cdk4 (Mm 01273583), Ccnd1 (Mm 00432359), Ccnd2 (Mm 00438071), and Ccnd3 (Mm 01273583).

In Vitro Cdk4 Kinase Assays—*In vitro* Cdk4 activity were performed as described previously (29). Four-week-old ST and DT mice were placed on vehicle or dox treatment in their drinking water for 3 weeks. After isolation, DT islets were cultured for 40 h in medium containing dox (2 μg/ml). Rapamycin (50 nM) or vehicle was added for 16 h before harvesting. Lysates from islets or MIN6 cells were immunoprecipitated using anti-Cdk4 antibody (Santa Cruz Biotechnology) and 50 μl of protein G-Sepharose beads (Sigma-Aldrich). The final kinase reaction was carried out in 50 mmol/liter HEPES, pH 7.5, 10 mmol/liter $MgCl_2$, 1 mmol/liter dithiothreitol, 2.5 mmol/liter EGTA 10 mmol/liter glycerophosphate, 0.1 mmol/liter Na_2VO_4, 1 mmol/liter NaF, 5 μmol/liter ATP, 6 mCi/reaction of [γ-^{32}P]ATP (Amersham Biosciences), and GST-Rb 769–921 (Santa Cruz Biotechnology). The samples were incubated at 30 °C for 30 min and separated by polyacrylamide gel electrophoresis. The amount of ^{32}P-labeled GST-Rb was visualized and quantified by autoradiography using a PhosphorImager. The levels of immunoprecipitated Cdk4 were used as loading control.

In Vitro Kinase Assay for Akt—Akt kinase activity was measured using the Akt kinase assay kit from Cell Signaling. Four-week-old ST and DT mice were placed on vehicle or dox treatment in their drinking water for 3 weeks. After isolation, ST and DT islets were cultured for 40 h with vehicle or dox (2 μg/ml), respectively. Rapamycin (50 nM) or vehicle was added for the last 16 h before harvesting. Resuspended immobilized Akt anti-

body slurry (20 μl) was added to 100 μg of lysates to selectively immunoprecipitate Akt by gentle rocking 2 h at 4 °C. The pellet was washed twice with 500 μl of 1× lysis buffer and twice with 500 μl of 1× kinase buffer (25 mM Tris, pH 7.5, 5 mM β-glycerol phosphate, 2 mM dithiothreitol, 0.1 mM Na_3VO_4, and 10 mM $MgCl_2$). The immunoprecipitated pellet was then incubated with 40 μl of 1× kinase buffer supplemented with 200 μM ATP and 1 μg of GSK-3 fusion protein for 30 min at 30 °C allowing immunoprecipitated Akt to phosphorylate GSK-3. The reaction was terminated with 20 μl of 3× SDS sample buffer. The samples were boiled for 5 min and loaded on 12% SDS-PAGE gel. Band intensity was quantified using National Institutes of Health ImageJ software (v1.3.8x). Input protein was used as control for quantification of the Akt activity levels. Akt-induced phosphorylation of GSK-3 was detected by Western blotting using phospho-GSK-3/($Ser^{21/9}$) antibody.

Pulse-Chase Analysis—Islets from four ST and four DT mice/time point were washed in Dulbecco's modified Eagle's medium without methionine and cysteine for 30 min at 37 °C. The islets were pulse-labeled for 30 min with [^{35}S]Protein labeling mix (PerkinElmer Life Sciences) at 280 μCi total/reaction and then washed with warm phosphate-buffered saline before being placed in complete Dulbecco's modified Eagle's medium containing a 100-fold excess of unlabeled methionine for 30 and 60 min (chase). For the rapamycin experiments, the islets were preincubated with 50 nM rapamycin for 90 min before the pulse, and the treatment was continued during the pulse for 30 min. Islet lysates from the pulse and the chase conditions were immunoprecipitated using anti-cyclin D2 antibody. The immunoprecipitates from all the conditions were washed and separated by SDS-PAGE and subsequently transferred to a polyvinylidene difluoride membrane. Immunoprecipitated proteins were visualized by autoradiography using a PhosphorImager (Amersham Biosciences). The pulse-label experiments in MIN6 cells were performed essentially using the same conditions described for the islet experiment. Immunoblotting for cyclin D2 was used as loading control. Quantitation of band intensity was performed as described for immunoblotting experiments.

Metabolic Studies—Fasting blood samples were obtained after overnight fasting from the tail vein. Glucose was measured on whole blood using AccuChek II glucometer (Roche Applied Science). Glucose tolerance tests were performed in 18-h fasted animals by injecting glucose (2 mg/g) intraperitoneally as described previously (25).

Statistical Analysis—The quantitative data are presented as the means ± S.E. from at least three independent experiments, five mice, or 100 islets, unless indicated. We used the Student's *t* test to compare independent means. A p value of <0.05 was considered statistically significant.

RESULTS

Development of an Inducible System to Activate Akt/mTOR Signaling in β-Cell—To determine the molecular mechanisms involved in β-cell G_1-S transition by the mTOR arm of Akt signaling, we developed a dox-inducible system. DT mice were generated by crossing mice expressing the tetracycline reverse transactivator under the control of the rat insulin promoter (RIP-rTTA) with mice expressing constitutive active Akt under the control of the tetracycline operator (tetOcaAkt) (23, 24). The control group for these experiments included mice containing the RIP-rTTA transgene only, but similar results were observed when compared with tetOcaAkt (ST). Immunoblotting for Akt showed that islets from DT mice treated with dox for 6 h exhibited a slight increase in Akt levels and activity assessed by phosphorylation of GSK3β on Ser^9 (Fig. 1*A*). Akt expression and levels of phospho-GSK3β were significantly increased in islets from DT mice treated with dox for 24 h (Fig. 1*A*). These results indicated that the expression of Akt1 transgene in β-cells is regulated in a DOX-dependent manner.

To induce Akt in β-cells from adult mice, 12-week-old mice were given doxycycline in their drinking water for 20 weeks. Intraperitoneal glucose tolerance tests before dox treatment showed no difference in glucose tolerance between ST and DT mice (Fig. 1*B*). Improved glucose tolerance in DT mice was observed as early as after 6 weeks of dox treatment (supplemen-

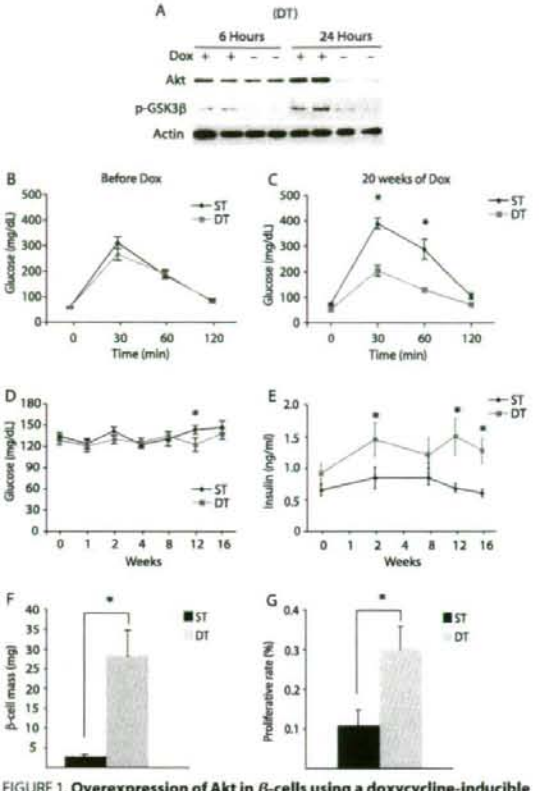

FIGURE 1. **Overexpression of Akt in β-cells using a doxycycline-inducible system.** *A*, immunoblotting for Akt and pGSK3α/β ($Ser^{21/9}$) in islets from ST (RIP-rtTA) and DT (RIP-rtTA/tetOcaAkt) mice treated with doxycycline for 6 and 24 h. *B*, intraperitoneal glucose tolerance test after overnight fasting in ST and DT mice before initiation of dox treatment. *C*, intraperitoneal glucose tolerance tests performed in ST and DT mice after 20 weeks of doxycycline treatment. *D*, 6-h fasting glucose measurements obtained from ST or DT mice. *E*, insulin levels in 6 h fasted ST and DT mice. *F*, β-cell mass measurements in ST and DT mice after 20 weeks on doxycycline or vehicle treatment. *G*, proliferation rate assessed by Ki67 in insulin-stained sections from ST and DT mice that received doxycycline treatment for 20 weeks. The data are presented as the means ± S.E. ($n = 5$). *, $p < 0.05$.

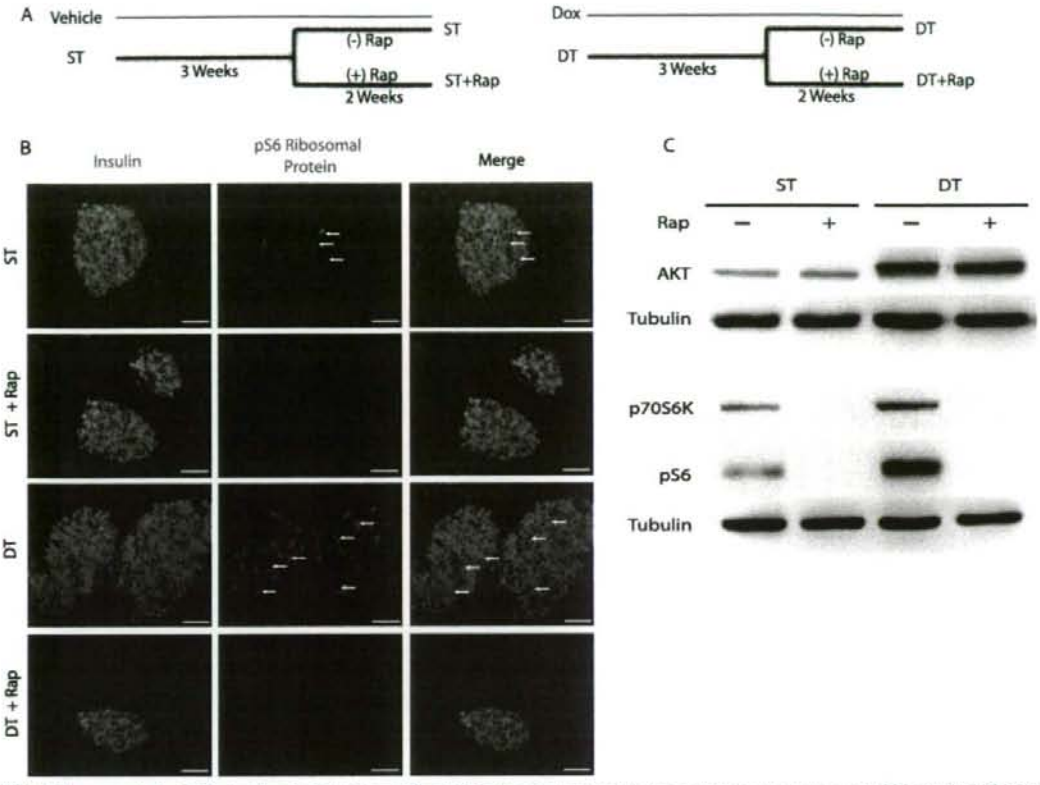

FIGURE 2. **Assessment of mTOR signaling in islets from ST and DT mice.** *A*, experimental design used to assess rapamycin effect on ST and DT mice. *B*, immunostaining for insulin (*green*) and pS6 ribosomal protein (*red*) in islets from ST and DT mice at the end of the experimental protocol. *C*, immunoblotting for total Akt, p70S6K (phospho-p70 S6K Thr 389), phospho-S6 ribosomal protein ($Ser^{235/236}$) (pS6) and tubulin in islet lysates from ST and DT mice at the end of the experimental protocol described in *A*. Islets from all groups were harvested immediately after isolation and subjected to immunoblotting. *Scale bar*, 50 μm.

tal Fig. S1). The improved glucose tolerance in DT mice was maintained after 20 weeks of dox treatment (Fig. 1*C*). Assessment of 6-h fasting glucose levels in ST and DT mice at different time points during dox treatment demonstrated that glucose levels in DT mice during doxycycline treatment were not different from those obtained from ST mice (Fig. 1*D*). Serum concentrations of insulin in DT mice increased after 2 weeks of dox administration (Fig. 1*E*). Compared with ST mice, insulin levels in DT mice remained elevated after 16 weeks of dox administration (Fig. 1*E*).

The histology of the pancreas and quantitation of β-cell mass were assessed by islet morphometry. After 20 weeks of doxycicline treatment, β-cell mass was augmented more than 5-fold in DT mice compared with ST mice (Fig. 1*F*). β-Cell proliferation by determined Ki67 immunostaining in insulin-stained pancreatic sections showed a 3-fold increased in proliferative rate in DT mice (Fig. 1*G*). These results showed that the inducible system could be used as a powerful tool to study the molecular mechanisms involved in cell cycle progression and β-cell mass under proliferative conditions induced by Akt.

Rapamycin Treatment Inhibits the Activation mTORC1 Signaling by Akt—The importance of the mTORC1 in the metabolic and morphologic phenotype observed in DT mice was assessed using the following experimental design (Fig. 2*A*): 1) 4-week-old ST and DT mice were placed on vehicle or dox treatment in their drinking water for 3 weeks. 2) After 3 weeks of dox treatment, rapamycin was injected intraperitoneally for 2 weeks in half of the ST and DT mice. The other half of the ST and DT mice continued vehicle and dox treatment (Fig. 2*A*). To assess the inhibition of mTOR signaling by rapamycin treatment in ST and DT mice, we performed immunofluorescence staining using anti-phospho-S6 ribosomal protein ($Ser^{235/236}$) antibody (pS6rp) (Fig. 2*B*). DT mice exhibited a significant increase in pS6rp staining when compared with ST mice (Fig. 2*B*). Staining for pS6rp in the pancreas from rapamycin-treated ST and DT mice was completely absent, suggesting that the dose of rapamycin was effective in inhibiting mTOR activation by Akt (Fig. 2*B*). To complement these studies, we performed immunoblotting in islet lysates from these mice. After dox administration, Akt levels were higher in DT compared with ST mice (Fig. 2*C*). Rapamycin treatment had no effect on Akt levels from ST or DT mice (Fig. 2*C*). Similar to the results shown on Fig. 2*B*, levels for pS6rp were higher in DT than ST mice. Rapamycin treatment of ST and DT mice completely abolished the phosphorylation of S6rp (Fig. 2*C*).

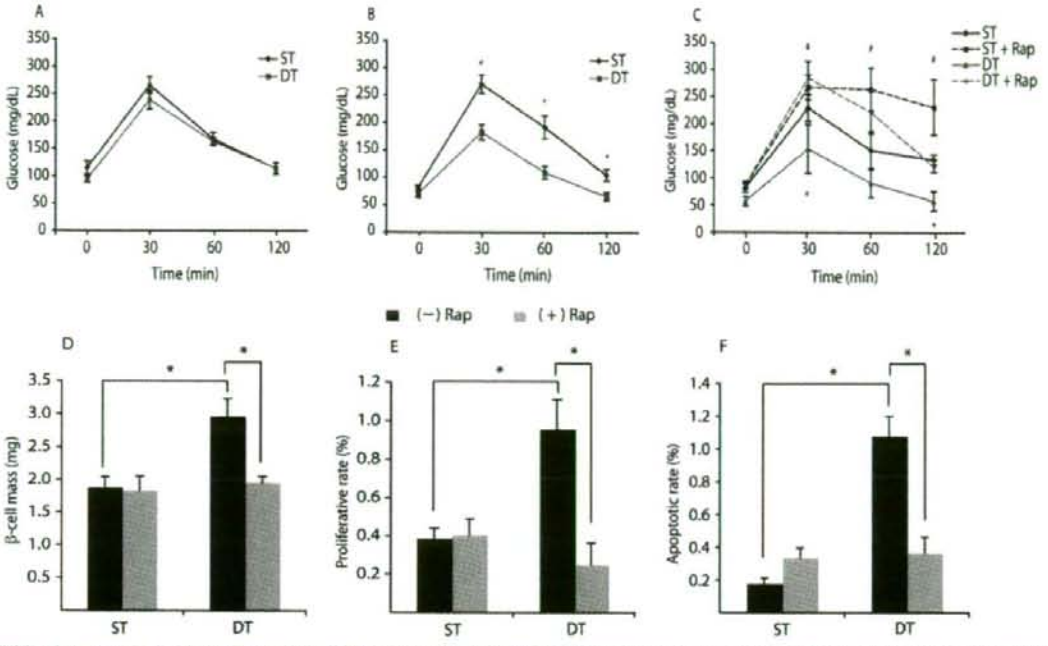

FIGURE 3. **Assessment of carbohydrate metabolism β-cell mass, proliferation, and apoptosis.** *A*, intraperitoneal glucose tolerance test after overnight fasting in ST and DT mice before initiation of dox treatment. *B*, after 3 weeks of doxycycline treatment. *C*, after 2 weeks of Rap treatment (5 mg/kg) daily. *D*, β-cell mass in ST and DT mice treated with vehicle or Rap (5 mg/kg) daily for 2 weeks as indicated in Fig. 2*A*. *E*, frequency of β-cell proliferation assessed by Ki67 staining in insulin-stained sections from ST and DT mice treated with vehicle or Rap (5 mg/kg) daily for 2 weeks as indicated in Fig. 2*A*. Co-staining for insulin and Ki67 defined proliferating cells. *F*, apoptosis measured by cleaved-caspase 3 staining in insulin-stained sections from ST and DT mice at the end of the experimental protocol described for Fig. 2*A*. Apoptotic cells were determined as cells that were co-stained for insulin and cleaved-caspase 3. The data are presented as the means ± S.E. ($n = 5$). *, $p < 0.05$; #, $p < 0.05$ DT + Rap *versus* DT.

Rapamycin Treatment Partially Reverses the Akt-mediated Improvement in Carbohydrate Metabolism—Assessment of carbohydrate metabolism in ST and DT mice treated with vehicle or rapamycin was then performed. Before administration of dox, glucose tolerance in 4-week-old ST and DT mice was comparable (Fig. 3*A*). In contrast to ST mice, DT mice treated with dox for 3 weeks exhibited lower glucose levels at 30, 60, and 120 min after glucose injection (Fig. 3*B*). Glucose tolerance after rapamycin treatment showed impaired glucose tolerance in ST+Rap mice when compared with ST mice (Fig. 3*C*). Glucose levels at 30, 60, and 120 min in DT+Rap mice were higher than those of DT mice treated with vehicle (Fig. 3*C*). Glucose tolerance in DT+Rap mice showed that glucose levels at 30 and 60 min were comparable with those of ST+Rap (Fig. 3*C*). The metabolic alterations induced by rapamycin treatment reversed after discontinuation of treatment (supplemental Fig. S2). These results indicate that the improvement in carbohydrate metabolism observed by activation of Akt in β-cells was partially reversed by the inhibition of the mTORC1.

Assessment of islet morphometry at the end of the experimental protocol showed that the β-cell mass in ST and ST+Rap mice was comparable (Fig. 3*D*). In contrast, the β-cell mass in DT mice was higher than that of ST mice (Fig. 3*D*; $p < 0.05$). Rapamycin treatment of DT mice reduced β-cell mass to the levels found in ST and ST+Rap (Fig. 3*D*). Proliferation assessed by Ki67 staining demonstrated that ST and ST+Rap exhibited similar rates of proliferation (Fig. 3*E*). The proliferative rate observed in DT mice was 2-fold greater than that of ST mice ($p < 0.05$; Fig. 3*E*). The increased proliferative rate observed in DT mice was completely inhibited by rapamycin treatment (Fig. 3*E*). Assessment of apoptosis by cleaved caspase 3 staining demonstrated that the apoptotic rate was increased in DT mice when compared with ST mice ($p < 0.05$; Fig. 3*F*). The apoptotic rate in DT mice was reduced by rapamycin treatment (Fig. 3*F*). Rapamycin treatment had no effect on apoptosis in ST mice (Fig. 3*F*). Taken together, these experiments suggest that overexpression of Akt in β-cells induces β-cell mass by increased proliferation in an mTORC1-dependent mechanism.

Rapamycin Treatment Had No Effect on mTORC2 and Akt Activity—Recent experiments suggest that the mTORC2 complex phosphorylates Akt on Ser^{473} (17). Although the mTORC2 complex was initially described as rapamycin-insensitive, recent evidence suggests that rapamycin treatment can modulate mTORC2 activity in some systems (30, 31). To test whether the effects of rapamycin treatment in β-cell mass and proliferation resulted from inhibition of mTORC2/Akt signaling, we assessed the phosphorylation status of Akt and Akt kinase activity in islets from ST and DT mice treated with vehicle or rapamycin. Phosphorylation of Akt on Thr^{308} was increased in islets from DT mice (Fig. 4*A*). Rapamycin treatment had no effect on phosphorylation of Akt on Thr^{308} in islets lysates from ST and DT mice (Fig. 4*A*). Similarly, Akt phosphorylation on

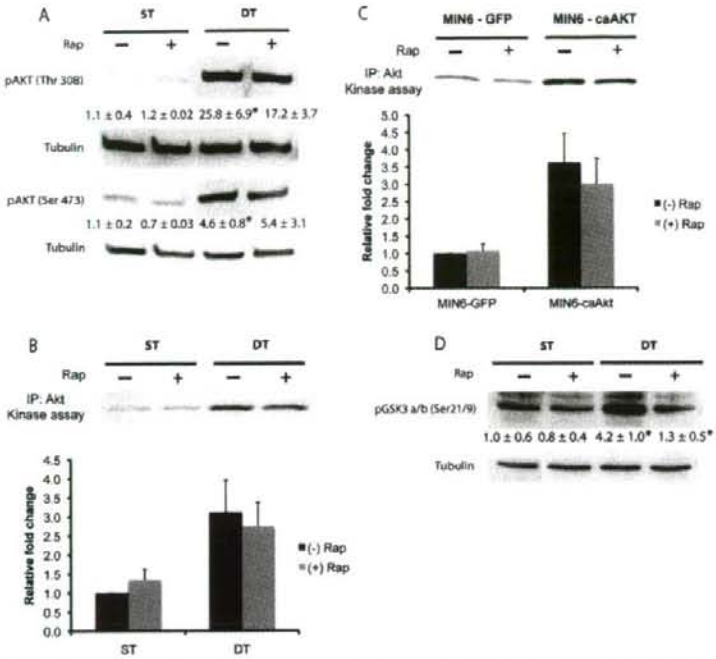

FIGURE 4. **Assessment of Akt activity.** *A*, immunoblotting for pAKT (Thr^{308}) and pAKT (Ser^{473}) in islets lysates from ST and DT mice treated with vehicle or 50 nM Rap. For these experiments, islets from dox-treated ST and DT mice were cultured in medium containing vehicle or dox for 40 h. Rapamycin was added to the culture for the last 16 h before harvesting. *B*, *in vitro* Akt kinase activity in islets from ST and DT mice subjected to the same experimental conditions described in *A* ($n = 4$). *C*, *in vitro* Akt kinase activity in MIN6 cells overexpressing constitutive active Akt ($n = 4$). The cells were cultured in the presence of vehicle or rapamycin (50 nM) for 16 h before harvesting. Quantification data from *in vitro* Akt kinase activity in islets and MIN6 cells is presented as fold change with respect to that of vehicle-treated control. *D*, immunoblotting for pGSK α/β (Ser 21/9) and tubulin as loading control in islets from ST and DT mice treated as described for *A*. The data are presented as the means ± S.E. ($n = 3$). *, $p < 0.05$.

Ser^{473} was increased in DT mice compared with ST mice, and these changes were not affected by rapamycin (Fig. 4*A*). *In vitro* Akt kinase activity in islets from ST and DT mice showed increased Akt kinase activity in DT mice (Fig. 4*B*). Akt activity in ST or DT mice was not altered by rapamycin (Fig. 4*B*). Similar to islets from ST and DT mice, *in vitro* Akt kinase activity was increased in MIN6 cells stably transfected with a constitutively active mutant of Akt (MIN6-caAkt), and this activity was not altered by rapamycin treatment (Fig. 4*C*). Phosphorylation of endogenous GSK3α/β on $Ser^{21/9}$ was increased in islet lysates from DT mice when compared with ST mice (4.2 ± 1.0, $p < 0.05$). In contrast to the *in vitro* Akt kinase activity, rapamycin treatment of DT islets inhibited the phosphorylation of GSK3α/β on $Ser^{21/9}$, suggesting that a downstream target of mTOR could phosphorylate GSK3α/β on the same residue as Akt (Fig. 4*D*; $p < 0.05$). These experiments suggest that rapamycin treatment did not alter the phosphorylation status or activity of Akt in islets or cell lines overexpressing a constitutively active form of Akt.

Rapamycin Treatment Inhibited Cdk4 Activity by Reducing Cyclin D2 and D3 Levels—The effect of rapamycin in β-cell proliferation in DT islets was further investigated by analysis of the cyclin D-Cdk4 complex. *In vitro* kinase activity assays were conducted using recombinant GST-Rb (amino acids 769–921) as substrate. This exogenous substrate contains the phosphorylation site for Cdk4. The incorporation of radioactive phosphate to this substrate is proportional to Cdk4 activity in the immunoprecipitate. The activity of Cdk4 in islets from DT mice was increased when compared with that of ST mice (Fig. 5*C*). The activation of Cdk4 observed in islets from DT mice was inhibited by rapamycin treatment (Fig. 5*C*; 1.4 + 0.1 *versus* 0.8 + 0.07, $p < 0.005$). Rapamycin also inhibited Cdk4 activity in islets from ST mice (Fig. 5*C*). No differences in the amount of immunoprecipitated Cdk4 among the different experimental conditions were observed (Fig. 5*C*, *lower panel*). The increased Cdk4 activity observed in islets from mice expressing a constitutively active form of Akt under the control of the insulin promoter (caAkt) was also inhibited by rapamycin (Fig. 5*A*). Similar inhibition of Cdk4 activity was obtained when MIN6 cells stably transfected with a caAkt mutant or GFP control were exposed to rapamycin treatment (Fig. 5*B*). Assessment of the cyclin D-Cdk4 complex components involved in regulation of Cdk4 activity showed that cyclin D2 and D3 but not D1 protein levels were increased in DT mice (3.1 ± 0.7 and 1.5 ± 0.1, respectively, $p < 0.05$) (Fig. 5*D*). Rapamycin treatment inhibited the induction of cyclin D2 and D3 in DT islets (Fig. 5*D*; $p < 0.05$). In contrast, cyclin D1 levels were not affected by rapamycin treatment of ST or DT islets (Fig. 5*D*). The levels of Cdk4 were no different among all the conditions (Fig. 5*D*). P27 levels in islets from DT mice were decreased when compared with those of ST mice (0.6 ± 0.1, $p < 0.05$). Rapamycin treatment had not effect on p27 levels in islets from both ST and DT mice (Fig. 5*D*). To assess cyclin D2 levels *in vivo*, we performed immunofluorescence staining in ST and DT mice treated and not treated with rapamycin (Fig. 5*E*). DT mice exhibited a significant increase in nuclear cyclin D2 staining when compared with ST mice (Fig. 5*E*). Staining for cyclin D2 in the pancreas from rapamycin-treated DT mice was absent, suggesting that mTORC1 regulates cyclin D2 protein levels.

Assessment of mRNA Levels of Cyclin D-Cdk4 Complex Components—Rapamycin treatment induced down-regulation of cyclin D2 and D3 in islets from DT mice (Fig. 5*D*). To determine whether the decrease in protein levels resulted from alterations in transcription, we performed real time PCR in islets from ST and DT mice treated with vehicle or rapamycin. Cyclin

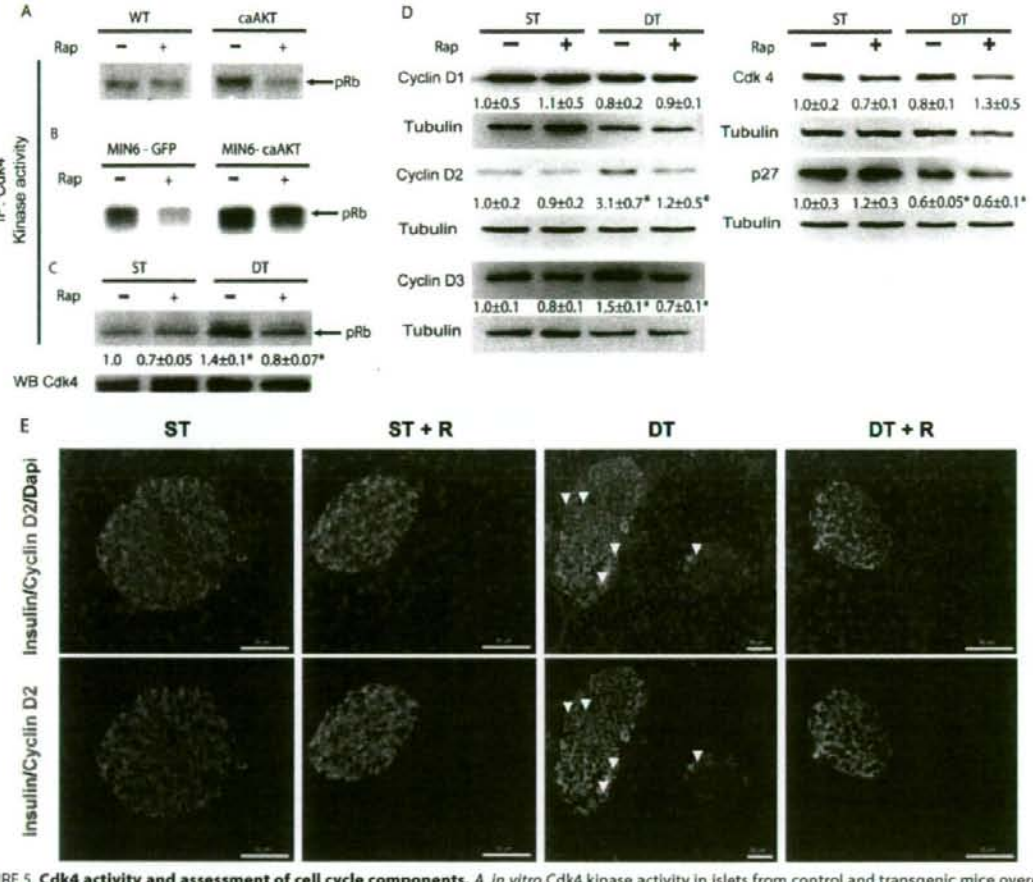

FIGURE 5. **Cdk4 activity and assessment of cell cycle components.** *A, in vitro* Cdk4 kinase activity in islets from control and transgenic mice overexpressing a constitutively active Akt under the rat insulin promoter (caAkt). The islets were cultured for 40 h after isolation, and Rap (50 nM) was included in the culture medium for the last 16 h of the culture. *B, in vitro* Cdk4 kinase activity in stable MIN6 cells overexpressing constitutively active Akt. MIN6-GFP and MIN6-caAkt were cultured in regular medium for 16 h in the presence of vehicle or rapamycin (50 nM). *C, in vitro* Cdk4 kinase activity in islets from ST and DT mice. The islets were obtained from ST or DT mice treated with vehicle or dox in the drinking water for 3 weeks. After isolation, the islets were cultured in medium with vehicle (ST) or dox (DT) for 40 h. Rapamycin (50 nM) or vehicle was added to the medium for the last 16 h of culture before harvesting. *D,* immunoblotting for cyclin D1, cyclin D2, cyclin D3, Cdk4, and p27 in islets from ST and DT mice treated and nontreated with rapamycin. These experiments were performed using the experimental protocol described for *C. E,* immunostaining for insulin (*green*) and cyclin D2 (*red*) in islets from ST and DT mice, treated, and nontreated with rapamycin using the experimental protocol described for Fig. 2*A*. The data are presented as the means ± S.E. ($n = 3$). *, $p < 0.05$.

D1 and D2 mRNA levels were reduced in islets from DT mice (Fig. 6). Rapamycin treatment of ST and DT islets resulted in induction of cyclin D1 and D2 levels when compared with those obtained from ST and DT islets. In contrast to cyclin D1 and D2, no changes among the different groups were observed for cyclin D3 (Fig. 6). Cdk4 mRNA levels were increased in DT mice compared with ST mice. Rapamycin treatment inhibited Cdk4 mRNA levels in DT mice (Fig. 6). p21 mRNA levels were no different between ST, ST+Rap, and DT islets. Islets from DT+Rap exhibited lower p21 mRNA levels when compared with those of DT islets (Fig. 6). Compared with islets from ST mice, p27 mRNA levels were decreased in islets from DT mice, and rapamycin had no effect (Fig. 6). These observations suggest that the increases in cyclin D2 and cyclin D3 levels observed in islets from DT mice occurred primarily by translational regulation and/or by an effect on protein stability.

Rapamycin Inhibits Cyclin D2 Synthesis—The reduction in cyclin D2 protein could be caused by a decrease in protein synthesis, a decrease in protein stability, or both. We therefore designed pulse-chase experiments to determine the rate of incorporation of radiolabeled methionine into cyclin D2 in the presence or absence of rapamycin treatment for 30 min (Fig. 7*A*). The pulse-labeling was followed by wash out (chase) for 1 h and subsequent immunoprecipitation with cyclin D2 antibodies. The rate of synthesis of cyclin D2 was elevated in islets from DT mice when compared with ST mice (Fig. 7*A*). Rapamycin treatment of DT islets inhibited the synthesis of cyclin D2 (Fig. 7*A*). The levels of cyclin D2 after 1 h of the chase were higher in

DT mice when compared with ST mice (Fig. 7*A*). Pulse-label experiments in MIN6 cells were performed to corroborate the islet data (Fig. 7, *B* and *C*). Rapamycin treatment inhibited cyclin D2 synthesis in control (MIN6-GFP) and in MIN6 cells expressing a constitutively active Akt (MIN6-caAkt) ($p < 0.05$). To confirm that activation of Akt signaling in DT islets regulates the stability of cyclin D2, we pulse-labeled islets from ST and DT mice for 1 h and performed a 30-min chase in the presence of cyclohexamide (Fig. 7*D*). Cyclin D2 levels in DT mice were higher after 30 min of culture with cyclohexamide, indicating that Akt regulates cyclin D2 stability (Fig. 7*D*).

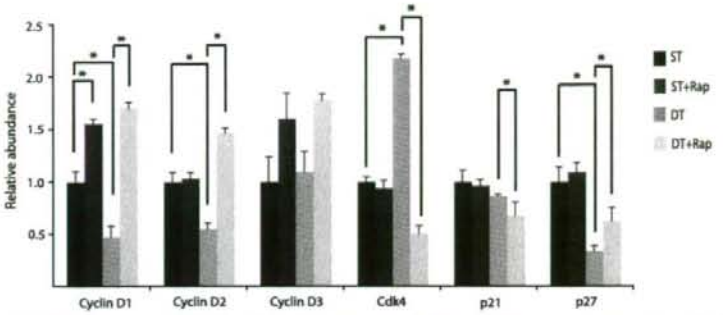

FIGURE 6. **Measurement of mRNA levels for G_1 components in islets.** TaqMan reverse transcription-PCR for cyclin D1, cyclin D2, cyclin D3, Cdk4 p21, and p27 in islets from ST and DT mice treated and nontreated with rapamycin. For these experiments, the islets were obtained from ST or DT mice treated with vehicle or dox in the drinking water for 3 weeks. After isolation, the islets were cultured in medium with vehicle (ST) or dox (DT) for 40 h. Rapamycin (50 nM) or vehicle was added to the medium for the last 16 h of culture before harvesting. The data are presented as the means ± S.E. ($n = 3$). *, $p < 0.05$.

Rapamycin Affects the Stability of Cyclin D2 and D3 Protein—The previous experiments indicated that activation of Akt signaling increases cyclin D2 stability. To assess whether the mTORC1 mediated the augmented cyclin D2 stability induced by Akt, the stability of this cyclin in islets from DT mice treated

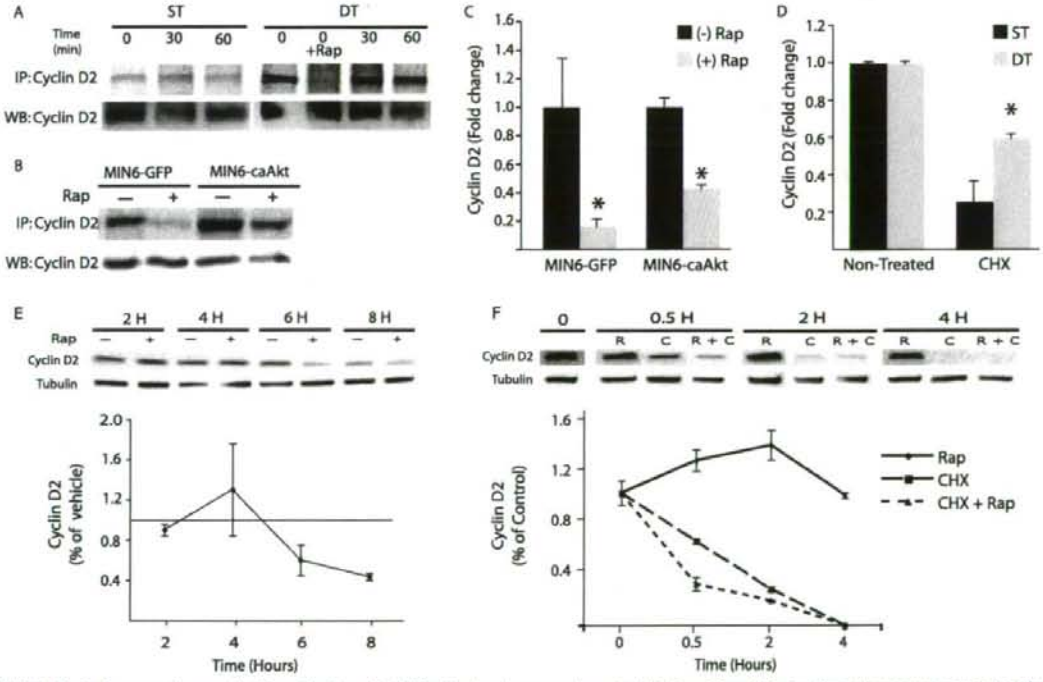

FIGURE 7. **Effect of rapamycin on cyclin D2 synthesis and stability.** *A*, pulse-chase experiment in islets from ST and DT mice. Protein lysates were precipitated with monoclonal antibody to Cyclin D2. Islets were treated with Rap (50 nM) as indicated under "Experimental Procedures." Immunoblotting for cyclin D2 was used as loading control. The blot is representative of two independent experiments. *B*, pulse-label experiment in control (MIN6-GFP) and MIN6 cells expressing a constitutively active Akt (MIN6-caAkt). MIN6 cells were preincubated with 50 nM rapamycin for 90 min before the pulse, and the treatment was continued during the pulse for 30 min. Immunoblotting for cyclin D2 was used as loading control. *C*, quantitation and statistical analysis of the pulse-label experiment performed in MIN6 cells (*B*). *D*, islets from ST and DT mice were treated with 12.5 μg/ml cycloheximide (*CHX*) for 30 min, and the levels of cyclin D2 were determined by immunoblotting. Protein bands for cyclin D2 were quantified and normalized to the levels in islets treated with vehicle control. *E*, islets from DT mice were treated with Me_2SO or 50 nM rapamycin for 2, 4, 6, and 8 h, and the levels of cyclin D2 were determined by immunoblotting. Protein bands for cyclin D2 were quantified, normalized to levels in DT mice treated with Me_2SO, and represented as the average of three separate experiments. *F*, islets from DT mice were treated with cycloheximide (*lanes C*) in the presence or absence of rapamycin (*lanes R*) for the indicated times. The levels of cyclin D2 were determined by immunoblotting. Protein bands for cyclin D2 were quantified, normalized to levels in DT mice before treatment, and represented as the average of three separate experiments. The data are presented as the means ± S.E. ($n = 3$). *, $p < 0.05$.

with control vehicle or rapamycin was determined (Fig. 7*E*). Compared with vehicle control, the levels of cyclin D2 were lower after 6 h of treatment with rapamycin (Fig. 7*E*). The decreased in cyclin D2 levels induced by rapamycin could be explained by reduction in protein synthesis or by decreased stability. To determine the effect of rapamycin treatment on cyclin D2 stability, we determined the half-life of cyclin D2 by treating islets from DT mice with cycloheximide for different times in the presence or absence of rapamycin (Fig. 7*F*). Similar to the results shown on Fig. 7*C*, cyclin D2 levels were not altered during the first 4 h of rapamycin treatment (Fig. 7*F*). In contrast, cyclin D2 was not detected after 4 h of treatment with cyclohexamide (Fig. 7*F*). Treatment with cycloheximide and rapamycin further decreased the cyclin D2 levels. Decrease in steady state levels of cyclin D3 were observed only after 6 h of rapamycin treatment (supplemental Fig. S3). In contrast to cyclin D2, cyclin D3 expression was not affected by cycloheximide treatment (supplemental Fig. S3). Treatment with cycloheximide and rapamycin further decreased the half-life of cyclin D3 protein. These results indicate that rapamycin affected cyclin D2 and D3 stability.

DISCUSSION

The current studies provide new insights into the molecular mechanisms that govern cell cycle and β-cell proliferation, a critical component for maintenance of β-cell mass. Here, we present evidence showing that mTORC1 signaling is a major modulator of β-cell expansion and cell cycle progression by regulating cyclin D2 and D3 levels and Cdk4 activity. These studies show for the first time that the mTORC1 modulates cyclin D2 synthesis and stability and suggest that the mTORC1 is an important component in post-transcriptional regulation of cell cycle components in β-cells. These observations are clinically relevant because they suggest that rapamycin has deleterious effects on β-cells. Rapamycin treatment may attenuate the adaptive responses of β-cells in patients with insulin resistance and in other states that require the expansion of β-cells. This work can positively affect treatment of human diabetes, because it uncovers potential targets to develop new pharmacologic agents designed to augment proliferation of β-cells *in vivo* and *in vitro*. In addition, the fundamental knowledge obtained on the role of the mTORC1 pathway in β-cell cycle progression provides a better understanding of the effects of immunosuppressant medications used in islet transplantation protocols and suggests that the use of rapamycin could negatively impact the success of islet transplantation.

The serine-threonine kinase Akt has been demonstrated to be an important mediator of growth signals in β-cells. Induction of Akt by dox administration resulted in progressive improvement in glucose tolerance and hyperinsulinemia as a result of increased β-cell mass and proliferation. The inhibition of mTORC1 signaling by rapamycin partially reverted the improved glucose tolerance induced by activation of Akt in β-cells. Interestingly, the effect of rapamycin in glucose tolerance was also observed in ST mice, suggesting that rapamycin alters insulin secretion and/or insulin sensitivity. We cannot discard the possibility of decreased glucose-stimulated insulin secretion by rapamycin in our model, but insulin levels in the fed state were comparable among the groups (data not shown). Insulin tolerance test demonstrated that rapamycin induced insulin resistance in ST mice (supplemental Fig. S4). The alterations of insulin sensitivity in DT mice were less apparent, because DT mice showed some degree of insulin resistance, perhaps as a response of chronic hyperinsulinemia (supplemental Fig. S4). Therefore, we can conclude that the reversal of the metabolic phenotype in rapamycin-treated DT mice could be explained in part by a combination of development of insulin resistance, inhibition of β-cell expansion, and possibly a component of altered insulin secretion. However, the expected adaptive response to insulin resistance would be an expansion of β-cell mass. In contrast, we observed a reduction in β-cell mass in rapamycin-treated DT mice for 15 days as a result of decreased proliferation, suggesting that the effect of rapamycin on β-cells is a major component of the phenotype. Rapamycin treatment was not associated to increased in apoptotic rate. Interestingly, DT mice exhibited augmented apoptosis most likely associated to increased proliferation and enhanced turnover. The changes in β-cell mass after of rapamycin could be explained by reduced cell size, because 15 days of treatment is a short time to observe an effect from inhibition of proliferation. It is also possible that the impaired glucose phenotype observed in rapamycin-treated ST and DT mice could be caused by alterations in β-cell function because rapamycin treatment has been shown to reduce mitochondrial potential and affect insulin secretion (32, 33).

Akt signaling regulates several downstream targets that regulate multiple biological processes. In these experiments, we used rapamycin to assess the role of mTORC1 in Akt signaling. Rapamycin has been used extensively in the literature as specific inhibitor of the mTORC1 complex. However, recent evidence suggests that rapamycin can also disturb the mTORC2 complex (31). Therefore, it was plausible that the rapamycin effect resulted solely from inhibition of Akt signaling. However, rapamycin treatment of islets from DT mice had no effect on phosphorylation of Akt in Ser^{473} and Thr^{308} and Akt activity. These observations suggest that in our *in vitro* experimental conditions, mTORC2 activity in β-cells was not altered by rapamycin treatment and that alterations in mTORC2 activity were not responsible for the rapamycin effects. These results are consistent with the concept that the mTORC1 is the major regulator of β-cell mass and proliferation in this system. The importance of the mTORC1 in β-cell proliferation and mass has also been demonstrated recently in mice conditionally deficient for Tsc2 in β-cells (βTsc2). In these mice, activation of mTOR signaling by deletion of Tsc2 in β-cells resulted in increased β-cell mass and proliferation, and these changes were completely suppressed by rapamycin treatment (22). Experiments using rapamycin in pancreatectomy models and pregnancy provide further evidence for a role of the mTORC1 in adaptive responses of β-cells to stress conditions. The results of the current experiments provide new insights into the importance of mTORC1 in proliferative conditions and unravel the mechanisms whereby inhibition of the mTORC1 regulates the cell cycle and mass in β-cells. The novel findings on the regulation of cyclin D2 synthesis and stability by the mTORC1 also provides critical information for the use of rapamycin in malig-

nancies and tissues in which cell cycle progression is driven mainly by increases in cyclin D2 and D3.

Previous studies suggest that modulation of the cyclin D-Cdk4 complex activity is a major step in controlling the cell cycle progression, proliferation, and maintenance of β-cell mass (27, 34–37). Genetic experiments indicated that cyclin D2 and to a lesser extent cyclin D1 are critical for maintenance of β-cell mass and proliferation post-natally (36, 38). In the current experiments, we showed mTORC1 activity regulates Cdk4 activity by modulation of cyclin D2 and D3 levels. The pulse-chase experiments showed that the activity of the mTORC1 plays an important role in regulation of cyclin D2 synthesis. The mechanisms involved in regulation of cyclin D2 synthesis by the mTORC1 are unclear, but it is possible that this complex favors the translation of cyclin D2 by regulating elements in the 5′- or 3′-untranslated region of the mRNA. In addition to synthesis, our observations showed for the first time that the mTORC1 also regulates the stability of cyclin D2 and D3 (Fig. 7*F* and supplemental Fig. S3). The mechanisms involved in this process are not entirely clear, but rapamycin treatment of islets from DT mice inhibited GSK3β phosphorylation. The inhibition in GSK3 phosphorylation could explain in part the reduction in cyclin D2 stability because activation of this kinase phosphorylates D-type cyclins and induces ubiquitin-proteosome-dependent degradation (39–43). The inhibition of GSK3β phosphorylation was surprising because it suggests that a downstream target of mTOR could phosphorylate GSK3β at the same residue as Akt. Interestingly, evidence in TSC2-deficient fibroblast demonstrated that S6K1 phosphorylates GSK3β on the site normally phosphorylated by Akt, and this was inhibited by rapamycin (44). Because the inhibition of GSK3β by rapamycin was observed in the context of constitutively activation of Akt, it is reasonable to conclude that S6K phosphorylation of GSK3 could be a more important mechanism. Future experiments with proteosome inhibitors will provide useful information to determine the mechanisms involved in cyclin D2 stability by Akt/mTORC1 signaling. In summary the current experiments suggest that the mTORC1 activity is a major regulator of the stability of cyclin D2 and D3 by regulation of GSK3β.

These studies uncovered key novel pathways controlling cell cycle progression in β-cells *in vivo*. This information can be used to develop alternative approaches to expand β-cell mass *in vivo* and *in vitro* without the risk of oncogenic transformation. The acquisition of such knowledge is critical for the design of improved therapeutic strategies for the treatment and cure of diabetes as well as to understand the effects of mTOR inhibitors in β-cell function. A better understanding of the effects of rapamycin in β-cells mass and function will be important to the advancement and improvement of the success of islet transplantation.

Acknowledgments—We thank Gerhard Christofori and Shimon Efrat for providing the RIP-rtTA mice. We acknowledge the support of the Radioimmunoassay, Morphology, and β-Cell Morphology cores from the Washington University Diabetes Research & Training Center. We also thank the Morphology core from Washington University Digestive Diseases Research Core Center for histology sections.

REFERENCES

1. Kahn, S. E. (2001) *J. Clin. Endocrinol. Metab.* **86,** 4047–4058
2. White, M. F. (2002) *Am. J. Physiol.* **283,** E413–E422
3. Bonner-Weir, S. (2000) *J. Mol. Endocrinol.* **24,** 297–302
4. Dor, Y., Brown, J., Martinez, O. I., and Melton, D. A. (2004) *Nature* **429,** 41–46
5. Kwon, G., Marshall, C. A., Liu, H., Pappan, K. L., Remedi, M. S., and McDaniel, M. L. (2006) *J. Biol. Chem.* **281,** 3261–3267
6. Kulkarni, R. N. (2005) *Rev. Endocr. Metab. Disord.* **6,** 199–210
7. Nielsen, J. H., Galsgaard, E. D., Møldrup, A., Friedrichsen, B. N., Billestrup, N., Hansen, J. A., Lee, Y. C., and Carlsson, C. (2001) *Diabetes* **50,** S25–29
8. Murakami, M., Ichisaka, T., Maeda, M., Oshiro, N., Hara, K., Edenhofer, F., Kiyama, H., Yonezawa, K., and Yamanaka, S. (2004) *Mol. Cell. Biol.* **24,** 6710–6718
9. Zhang, Y., Gao, X., Saucedo, L. J., Ru, B., Edgar, B. A., and Pan, D. (2003) *Nat. Cell Biol.* **5,** 578–581
10. Garami, A., Zwartkruis, F. J., Nobukuni, T., Joaquin, M., Roccio, M., Stocker, H., Kozma, S. C., Hafen, E., Bos, J. L., and Thomas, G. (2003) *Mol. Cell* **11,** 1457–1466
11. Inoki, K., Li, Y., Xu, T., and Guan, K. L. (2003) *Genes Dev.* **17,** 1829–1834
12. Inoki, K., Li, Y., Zhu, T., Wu, J., and Guan, K. L. (2002) *Nat. Cell Biol.* **4,** 648–657
13. Manning, B. D., Tee, A. R., Logsdon, M. N., Blenis, J., and Cantley, L. C. (2002) *Mol. Cell* **10,** 151–162
14. Sarbassov, D. D., Ali, S. M., Kim, D. H., Guertin, D. A., Latek, R. R., Erdjument-Bromage, H., Tempst, P., and Sabatini, D. M. (2004) *Curr. Biol.* **14,** 1296–1302
15. Jacinto, E., Loewith, R., Schmidt, A., Lin, S., Ruegg, M. A., Hall, A., and Hall, M. N. (2004) *Nat. Cell Biol.* **6,** 1122–1128
16. Harris, T., and Lawrence, J. C. (2003) *Science STKE* **212,** 1–17
17. Sarbassov, D. D., Guertin, D. A., Ali, S. M., and Sabatini, D. M. (2005) *Science* **307,** 1098–1101
18. Shima, H., Pende, M., Chen, Y., Fumagalli, S., Thomas, G., and Kozma, S. C. (1998) *EMBO J.* **17,** 6649–6659
19. Um, S. H., Frigerio, F., Watanabe, M., Picard, F., Joaquin, M., Sticker, M., Fumagalli, S., Allegrini, P. R., Kozma, S. C., Auwerx, J., and Thomas, G. (2004) *Nature* **431,** 200–205
20. Ruvinsky, I., Sharon, N., Lerer, T., Cohen, H., Stolovich-Rain, M., Nir, T., Dor, Y., Zisman, P., and Meyuhas, O. (2005) *Genes Dev.* **19,** 2199–2211
21. Shigeyama, Y. K. T., Kido, Y., Hashimoto, N., Asahara, S. I., Matsuda, T., Takeda, A., Inoue, T., Shibutani, Y., Koyanagi, M., Uchida, T., Inoue, M., Hino, O., Kasuga, M., and Noda, T. (2008) *Mol. Cell. Biol.* **28,** 2971–2979
22. Rachdi, L., Balcazar, N., Osorio-Duque, F., Elghazi, L., Weiss, A., Gould, A., Chang-Chen, K. J., Gambello, M. J., and Bernal-Mizrachi, E. (2008) *Proc. Natl. Acad. Sci. U. S. A.* **105,** 9250–9255
23. Milo-Landesman, D., Surana, M., Berkovich, I., Compagni, A., Christofori, G., Fleischer, N., and Efrat, S. (2001) *Cell Transplant* **10,** 645–650
24. Shiojima, I., Sato, K., Izumiya, Y., Schiekofer, S., Ito, M., Liao, R., Colucci, W. S., and Walsh, K. (2005) *J. Clin. Investig.* **115,** 2108–2118
25. Bernal-Mizrachi, E., Wen, W., Stahlhut, S., Welling, C. M., and Permutt, M. A. (2001) *J. Clin. Investig.* **108,** 1631–1638
26. Bernal-Mizrachi, E., Wice, B., Inoue, H., and Permutt, M. A. (2000) *J. Biol. Chem.* **275,** 25681–25689
27. Fatrai, S., Elghazi, L., Balcazar, N., Cras-Meneur, C., Krits, I., Kiyokawa, H., and Bernal-Mizrachi, E. (2006) *Diabetes* **55,** 318–325
28. Girish, V., and Vijayalakshmi, A. (2004) *Indian J. Cancer* **41,** 47
29. Matsushime, H., Quelle, D. E., Shurtleff, S. A., Shibuya, M., Sherr, C. J., and Kato, J. Y. (1994) *Mol. Cell. Biol.* **14,** 2066–2076
30. Sarbassov, D., Ali, S., Sengupta, S., Sheen, J., Hsu, P., Bagley, A., Markhard, A., and Sabatini, D. M. (2006) *Mol. Cell* **22,** 159–168
31. Zeng, Z., dos Sarbassov, D., Samudio, I. J., Yee, K. W., Munsell, M. F., Ellen Jackson, C., Giles, F. J., Sabatini, D. M., Andreeff, M., and Konopleva, M. (2007) *Blood* **109,** 3509–3512
32. Edinger, A. L., and Thompson, C. B. (2002) *Mol. Biol. Cell* **13,** 2276–2288
33. Zhang, N., Su, D., Qu, S., Tse, T., Bottino, R., Balamurugan, A. N., Xu, J.,

Bromberg, J. S., and Dong, H. H. (2006) *Diabetes* **55,** 2429–2436
34. Rane, S. G., and Reddy, E. P. (2000) *Front. Biosci.* **5,** D1–D19
35. Kiyokawa, H., Kineman, R. D., Manova-Todorova, K. O., Soares, V. C., Hoffman, E. S., Ono, M., Khanam, D., Hayday, A. C., Frohman, L. A., and Koff, A. (1996) *Cell* **85,** 721–732
36. Kushner, J. A., Ciemerych, M. A., Sicinska, E., Wartschow, L. M., Teta, M., Long, S. Y., Sicinski, P., and White, M. F. (2005) *Mol. Cell. Biol.* **25,** 3752–3762
37. Cozar-Castellano, I., Takane, K. K., Bottino, R., Balamurugan, A. N., and Stewart, A. F. (2004) *Diabetes* **53,** 149–159
38. Georgia, S., and Bhushan, A. (2004) *J. Clin. Investig.* **114,** 963–968
39. Diehl, J. A., Cheng, M., Roussel, M. F., and Sherr, C. J. (1998) *Genes Dev.* **12,** 3499–3511
40. Diehl, J. A., Zindy, F., and Sherr, C. J. (1997) *Genes Dev.* **11,** 957–972
41. Casanovas, O., Jaumot, M., Paules, A. B., Agell, N., and Bachs, O. (2004) *Oncogene* **23,** 7537–7544
42. Naderi, S., Gutzkow, K. B., Lâhne, H. U., Lefdal, S., Ryves, W. J., Harwood, A. J., and Blomhoff, H. K. (2004) *J. Cell Sci.* **17,** 3769–3783
43. Kida, A., Kakihana, K., Kotani, S., Kurosu, T., and Miura, O. (2007) *Oncogene* **26,** 6630–6640
44. Zhang, H. H., Lipovsky, A. I., Dibble, C. C., Sahin, M., and Manning, B. D. (2006) *Mol. Cell* **24,** 185–197